The many facets of RuII(dppe)2 acetylide compounds

Olivier Galangau, Stéphane Rigaut

Chemistry–A European Journal
Review
doi.org/10.1002/chem.202402788
Chemistry Europe
European Chemical Societies Publishing
www.chemeurj.org

The Many Facets of $Ru^{II}(dppe)_2$ Acetylide Compounds

Stéphane Rigaut*[a] and Olivier Galangau*[a]

In this contribution, we describe the various research domains in which Ru^{II} alkynyl derivatives are involved. Their peculiar molecular properties stem from a strong and intimate overlap between the metal centered d orbitals and the π system of the acetylide ligands, resulting in plethora of fascinating properties such as strong and tunable visible light absorption with a strong MLCT character essential for sensing, photovoltaics, light-harvesting applications or non-linear optical properties. Likewise, the d/π mixing results in tunable redox properties at low potential due to the raising of the HOMO level, and making those compounds particularly suited to achieve redox switching of various properties associated to the acetylide conjugated ligand, such as photochromism, luminescence or magnetism, for charge transport at the molecular level and in field effect transistor devices, or charge storage for memory devices. Altogether, we show in this review the potential of Ru^{II} acetylide compounds, insisting on the molecular design and suggesting further research developments for this class of organometallic dyes, including supramolecular chemistry.

1. Introduction

Transition metal alkynyl derivatives have attracted a great deal of attention over the last decades and became key motifs in numerous research fields for material applications. For instance, these metal complexes, as well as their oligomers or polymers, have shown promising properties in linear and Non-Linear Optics (NLO),[1] as organometallic semiconducting materials for photovoltaics and OLEDs.[2] They were also thoroughly investigated as molecular wires for charge transport at the molecular scale.[3] Alternatively, the metal center may also contribute to the formation of supramolecular assemblies, granting these molecules with Liquid Crystal (LC) behavior or solution state self-assembly abilities.[4] Finally, their biomedical applications were also recently reviewed.[5]

In general, the insertion of a metal atom into a π-conjugated system endows acetylide compounds with superior (opto)-electronic properties compared to their metal-free analogs. In such complexes, the frontiers orbitals of the organic ligands and the d-centered orbitals lead primarily to σ bond formation but also to π-type lateral overlapping. The resulting antibonding molecular orbitals display a mixed d-π character which depends on the relative energy levels of the metal and the organic fragments orbitals. This π-type overlapping is therefore characteristic of the complex's HOMO orbital.

In other words, varying the nature of the π system, the nature of the metal produces electronic structures with a balanced proportion of d and/or π character of outmost importance in order to control the molecule's electronic properties.

As an illustration, group 10 Pt^{II} -acetylide derivatives have become ubiquitous in the field of organic electronics and they were shown to be successful molecules to design OPV and OFET devices.[2a,6] However, these compounds are typically not redox active because of a limited d/π mixing, whereas group 6–8 metal-acetylide compounds are redox active and have exhibited electron delocalization to different extents thanks to stronger d/π orbital overlap.[3a] In particular, Ru^{II} acetylides of the type [Ru]–C≡C–R display exceptionally high π characters balanced with d orbitals at their HOMO level, with respect to other metals, making them appealing molecular materials for the development of more efficient optoelectronic devices.[3a,7] Of particular interest are the $Ru^{II}(dppe)_2$ (bis–)acetylide compounds (dppe = 1,2-diphenylphosphine ethane) as (i) they are robust complexes stable in air, (ii) they can readily be obtained in high yields thanks to a methodology established by Touchard[8a] and Raithby[8b] from *cis*-$Ru(dppe)_2Cl_2$, and (iii) Mono and bis-acetylide compounds could be generated as well as symmetric or non-symmetric molecules in order to achieve insertion of this fragment in any organic conjugated path in contrast to the "end-cap only" CpRu(dppe) systems or its analogues. For interested readers, synthetic methodologies of $Ru^{II}(dppe)_2$acetylide derivatives, out of the scope of the present review, were recently reviewed by Ren and co-workers[9] and Low and co-workers.[10]

Altogether, the ease of synthesis of Ru alkynyl molecules, their adaptable structural and electronic properties allowing a fine-tuning of their optoelectronic and redox features make them appealing and versatile building block for functional materials. Therefore, in the following, we will review the various developments for specific properties and applications involving $Ru^{II}(dppe)_2$ acetylides, emphasizing the key roles of the molecular design and of the metal. Consequently, fundamental investigations of the electronic delocalization, as in case of mixed valence compounds, are out the scope of the present studies.[7a]

[a] S. Rigaut, O. Galangau
Univ. Rennes, CNRS, ISCR (Institut des Sciences Chimiques de Rennes)-UMR 6226 35000 Rennes, France
E-mail: stephane.rigaut@univ-rennes.fr
olivier.galangau@univ-rennes.fr

More precisely, we compiled a large list of various fundamental and practical research examples in which the Ru(II) acetylide tool was used to demonstrate several proofs of concept. As a matter of fact, although these compounds were known for more than 30 years, to our knowledge a review providing a global overview of their use and showing this building block's versatility is yet to be published. We believe it is only by exploring and confronting the many uses of Ru(II) acetylides that new molecular designs featuring innovative properties may emerge from this tool of constant importance.

The review is divided as follows. In the first part, we will focus on the benefit provided by these acetylides on linear and non-linear optical properties. Then, we will describe how they can promote unique electro- or photo- switching properties when associated with specific functional units. In a third part, their abilities to achieve charge storage or charge transport at the nanoscale will be considered. Finally, we will highlight the recent developments to achieve supramolecular assemblies.

2. Optical Properties of Ru(II) Acetylides Compounds

Ru^{II} alkynyl derivatives usually exhibit optical transitions in the visible and in the UV range of the electromagnetic spectrum. While the absorption bands located at high energies are mainly due to transitions involving the ancillary ligands,[11] the absorption bands located in the visible range or just below features extinction coefficients of $\sim 10^4\,L\,mol^{-1}\,cm^{-1}$ and are classically assigned to a d/π to π* electronic transitions, referred as MLCT bands due to their marked charge transfer character. These later electronic transitions have been the focus of many fundamental and practical investigations.

2.1. Tuneable Linear Optical Properties for Photovoltaic Applications

Because of their characteristic absorption MLCT bands, Ru(II) alkynyl compounds were designed for Dye Sensitized Solar Cells (DSSCs) and for Bulk HeteroJunctions solar cells (BHJs). In 2011, Colombo, Falciola and Luzzati[12] reported on the only example of BHJs with a rod-like bimetallic species exhibiting a Donor-Acceptor-Donor scaffold, where the donor is a *Chloro*-Ru complex and the acceptor a benzothiadiazole unit flanked on the two sides by thienyl moieties. The final molecule exhibited promising properties in solution, with a first optical transition located at 633 nm matching well with the sunlight spectrum. Unfortunately, the final BHJs device yielded only poor photovoltaic performances, with a Power to Conversion Efficiency (PCE) of 0.1%, assigned to the poor films morphology upon mixing with PCBM ([6,6]-phenyl-C_{61}-butyric acid methyl ester) leading to a strong phase segregation impeding both charge photogeneration and transport to the electrode. In 2014, Olivier and Toupance[13] fabricated the first TiO_2-based DSSC entailing a rod-like monometallic dipolar bis-alkynyl derivative, where the Ru center bridges electron donating phenyl carbazole unit to an electron withdrawing phenyl cyano-acrylic moiety (Figure 1). The compound exhibited a visible absorption located at 520 nm ($\varepsilon = 31\,000\,L\,mol^{-1}\,cm^{-1}$) in solution, but a sizeable blueshift of 50 nm assigned to deprotonation of the anchoring carboxylic acid was observed upon grafting on TiO_2 electrode. With such a simple design, an impressive PCE of 7.3% was achieved and the corresponding solar cell was stable for several weeks under ambient conditions showing how robust Ru alkynyl derivatives can be.

Inspired by this work, Colombo, Biagini and De Angelis replaced the carbazole donor group by a styryl-triphenyl amine one.[14] As a result, the final molecule has shown a limited redshift of the lowest transition (428 nm) compare to the previous one, leading further to a poor PCE of 1.5%. These examples underline how subtle can be the change of the donor moiety into these *push-pull* systems. Later on, Olivier and Toupance systematically investigated the importance of changing the acceptor moiety within D–Ru-A molecules where the donor was kept as a carbazole group (Figure 2).[15] Introducing a rhodanine, a bithiophene or a benzothiadiazole motif induced a marked redshift of the d/π-π* transition from 521 nm–659 nm. Interestingly, the best PCE of 7.1% was obtained with the bithiophene motif. They eventually improved the PCE to 7.49% by fabricating a mixed DSSC incorporating a 4:1 molar ratio of their original molecule and the bithiophene one providing a panchromatic absorption.

P-type DSSC where the semiconductor, usually NiO, is sensitized with a dye through a hole photoinjection is also a hot research topic. Because of their *push-pull* character and strong absorption, Olivier and Odobel[16] designed Ru-centered

Stéphane Rigaut receieved his Ph.D. from the University Bordeaux 1 in 1997, under the supervision of Prof. Didier Astruc and Dr. Marie hélène Delville. Following a postdoctoral training with Larry Miller at the University of Minnesota, he joined the universty of Rennes 1 in 1998 as an Assistant Professor and was promoted Full Professor in 2008. His research interests are focused toward metal complexes complexes for functionnal molecular materials and molecular electronics.

Olivier Galangau obtained his PhD in chemistry in 2011 from École Normale Supérieur de Cachan, under the supervision of Prof. P. Audebert. Following his postdoctoral training with Prof. T. Kawai at NAIST (Japan) he moved to Institut des Sciences Chimiques de Rennes (France) working with Dr. F. Pointillart. Since October 2018, he joined the group of Stéphane Rigaut as CNRS research fellow. He is interested in developing new types of smart molecular/supramolecular materials, combining light- and/or electro-switchability.

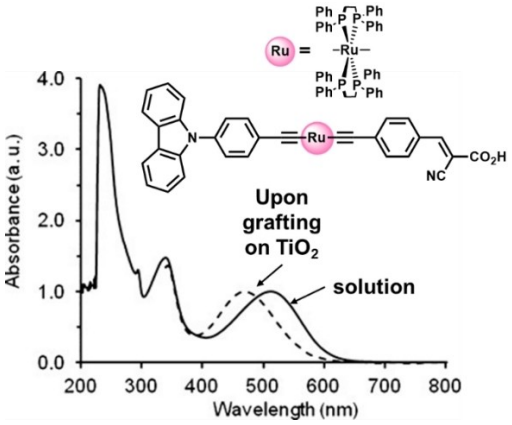

Figure 1. Organometallic D–Ru-A derivative developed by Olivier and Toupance. Adapted with permission from ref.[13] Copyright: 2014, Wiley-VCH.

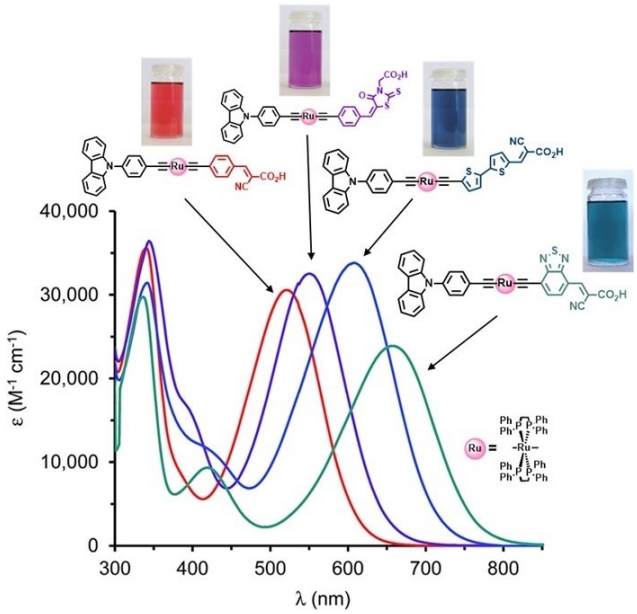

Figure 2. Variation of the MLCT band from visible to NIR ranges with different acceptor moieties. Adapted with permission from ref.[15] Copyright 2015, Royal Society of Chemistry.

alkynyl compounds endowed with a triphenylamine carboxylic acid on one side and on the other a bithiophene motif functionalized with an electron withdrawing group (acrylic ester or rhodamine). However, a moderate injection driving force combined to a low dye loading onto the NiO surface resulted in poor PCE. NiO-DSSc were further used as photocathodes in aqueous media for water splitting applications. Olivier and Artero[17] proposed a molecular design based on a Ru centered organometallic mixed alkynyl-allenylidene motif. Their design led to cationic organometallic dyes endowed with absorption spanning the entire visible and UV range, with a broad d/π to π*(allenylidene) transition. The compounds showed promising sizeable photocurrent density in view of their use in photo-electrochemical cell. Moreover, these organometallic dyes have shown excellent photostability under illumination, at pH 7 that also places them as promising sensitizers for photoelectrodes for H_2 evolution. Altogether, these examples demonstrate the tunability of the optical bandgap of Ru-alkynyl derivatives. Note that one of them display weak but sizeable absorption in the near infrared region.

In attempt to produce low-bandgap polymers, Cheng and Zhu recently combined Bodipy motifs to Ru bis-acetylide complexes.[18] Through an elegant "chemistry on the complex" approach, thanks to Sonogashira cross-coupling reactions, they obtained tetramers in excellent yields (Scheme 1). These oligomers exhibited an MLCT band located at 634 nm (653 nm) in solution (in films). This work demonstrates that Ru alkynyl spectroscopic properties can be tailored by using an oligomerization approach.

2.2. Linear Optical Properties: Sensing Applications

The tuning of optical bandgap of Ru alkynyl dyes has long been the center of intense research. In 2005, Fillaut[19] reported on a Ru-alkynyl complex appended with a barbituric moiety that exhibited d/π -π* optical transition located between 543–599 nm with very unusual solvatochromism (Figure 3). By comparing with the methylated reference molecule, the authors suggested that upon H-bonding with a H-acceptor solvent, the electron density on the acetylide ligand likely increased, which in turn partly reduced the MLCT character of the transition leading to strong blue shifts. Later, the blue shift being diagnostic of H-bonding interactions, the same group devel-

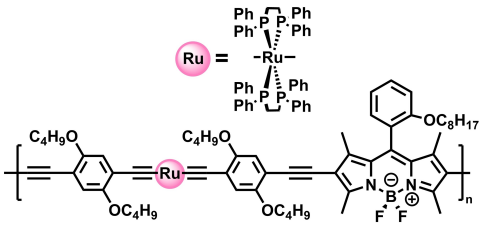

Scheme 1. 1,2-dppe Ru alkynyl oligomers (n = 4) with Bodipy motifs. Adapted with permission from ref.[18] Copyright, Copyright © 2014 Wiley Periodicals, Inc.

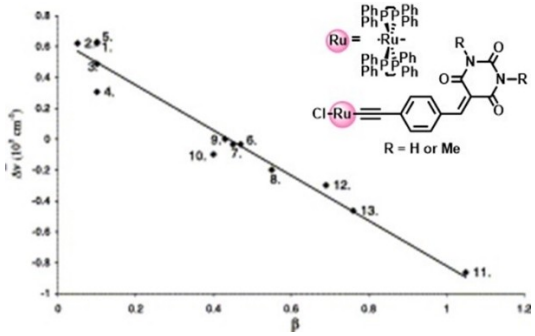

Figure 3. Correlation between the solvent hydrogen bond acceptor ability (β) and the calculated values $\Delta\nu$ ($cm^{<M-■1}$) = $\nu_{R=H}$ - $\nu_{R=Me}$. 1. CCl_4, 2. TCE, 3. $CHCl_3$, 4. DCE, 5. CH_2Cl_2, 6. Diethylether, 7. EtOAc, 8. THF, 9. Acetone, 10. MeCN, 11. HMPA, 12. DMF, 13. DMSO. Adapted with permission from ref.[19] Copyright[20]02 Elsevier Science B.V.

oped supramolecular optical (anion)sensors based on the interaction between an anion and their barbituric complexes (Figure 4).[20] They discovered that their optical (thio)barbituric-based probes were sensitive to F^- anions with affinity constants much superior for F^- versus AcO^- or H_2PO4^-. The colorimetric sensors experienced impressive blue shift from 590 nm–480 nm upon addition of the analyte ascribed to a deprotonation of the H atoms located on the barbituric head by the anions. However, deprotonation with piperidine did not lead to the same optical results.

By means of theoretical calculations, they eventually elucidated that the nature of the shift, upon F^- complexation, does not correspond to a change of frontier orbital energy, but should rather be related to a change in the nature of the orbital involved into the optical transition due to the point charge effect of the anion. It is worth noting that, Yagai and co-workers[21] recently demonstrated that organic molecules appended with barbituric moieties were prone to form supramolecular rosettes. The formation of such objects through cyclic hydrogen bonds has never been reported for Ru-alkynyl nor investigated but one might envisage that the initial observation of Fillaut and co-workers might be due to (partial) formation of supramolecular entities. It is worth noting that in light of recent supramolecular developments, variation of the optical properties of the organometallic fragment is an ideal method to investigate their self-assembly mechanism.

In a final study, Fillaut and co-workers used Ru-acetylides molecules appended with a flavonol moiety to detect lead ions in solution.[22] Upon chelation of Pb^{2+}, the absorption spectrum experiences a major bathochromic shift, as well as the typical fluorescence emission of the flavonol unit. Interestingly, the emission quantum yield drops concomitantly from 0.02 down to 0.008. This study highlighted that Ru alkynyl derivatives when properly decorated can also be used to detect metal traces.

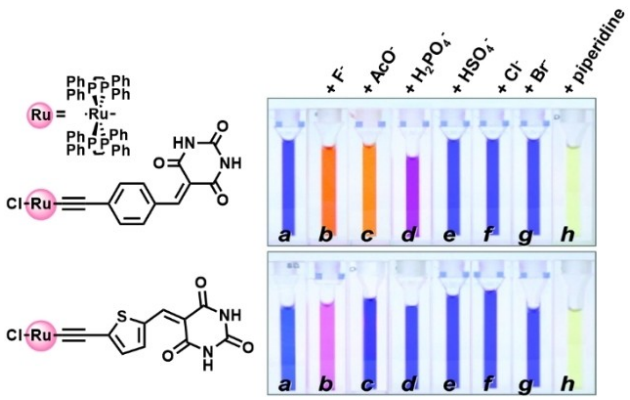

Figure 4. Naked-eye detection of anionic analytes by supramolecular interaction (solvent = CH_2Cl_2). Adapted with permission from ref.[20] Copyright 2005, Royal Society of Chemistry.

2.3. Nonlinear Optical Properties

Nonlinear optical (NLO) effects usually arise from the interaction between a high-intensity light beam (laser) and matter, resulting in a polarization of the material. Such a polarization produces in turn new electromagnetic fields that are altered in phase, frequency, amplitude and direction.[23] Two main NLO effects have been intensively studied over the past 50 years. The first one is related to the phenomenon called Second Harmonic Generation (SHG), which allows a frequency doubling of the incident light through the interaction of three waves within the NLO material, and is a 2nd order NLO effects through the measurement of the quadratic hyperpolarizability β. SHG has found applications in various domains such as in bioimaging, providing new perspectives in cancer research.[24] The second is a 3rd order NLO effects through the evaluation of the cubic hyperpolarizability γ that embraces a large variety of NLO processes, including the simultaneous absorption of several photons, providing power limiting protection equipment, NIR bioimaging, or valuable tool for 3D microfabrication.[25]

Derivatives encompassing a metal atom within the π conjugated path have proved their superior NLO character compared to intensively investigated organic counterparts,[26] especially those featuring push-pull dipolar π-conjugated systems. In particular, metal-alkynyl molecules (Metal = Pt, Au, Ru…) tend to display inherent MLCT character, which is at the origin of their exceptional NLO properties. Because in Ru-alkynyl complexes the d/π overlapping is strong, these derivatives were thoroughly investigated and literature studies clearly showed they outperformed other metal-acetylides compounds.[1,27f–k] In the following, we will only summarize the past key results and the most recent exciting achievements.

2nd order NLO studies. Humphrey and co-workers largely contributed to the field by investigating the 2nd order NLO properties of Ru alkynyl complexes.[1,27] They clearly demonstrated in rod-like dipolar *push-pull* Ru monoacetylide compounds that their MLCT character indeed produced strong 2nd order NLO response, and identified the nitro group ($-NO_2$) as the most effective to maximize the quadratic hyperpolarizability as well as the length of the π manifold (leading to greater π delocalization). They further observed that the *trans-ene* linkage instead of *yne* linkages in long acetylide ligands leads to small β value. Interestingly, the highest β value was obtained for a mixed *trans-ene*/*yne* ligand where the *trans-ene* linker was adjacent to the metal-bound phenyl-ethynyl moiety for raisons that remain unclear. De Angelis, Dragonetti and co-workers[28] later utilized rod-like bimetallic Ru alkynyl molecules to generate SHG signal (Scheme 2). The compound displayed impressive $\mu\beta_{EFISH}$ (where μ stands for the molecular dipole moment and β the quadratic hyperpolarizability) of -900 10^{-48} esu and -1370 10^{-48} esu at 1.907 μm as evaluated by the EFISH technic. The same group further improved the $\mu\beta_{EFISH}$ to -1550 10^{-48} esu and -1700 10^{-48} esu with monometallic dipolar molecules featuring a strong push-pull character.

Gauthier, Achelle and co-workers[29] markedly enhanced the $\mu\beta_{EFISH}$ with monometallic compounds where the metal is connected to a γ-pyranylidene donor moiety and a pyrimidine

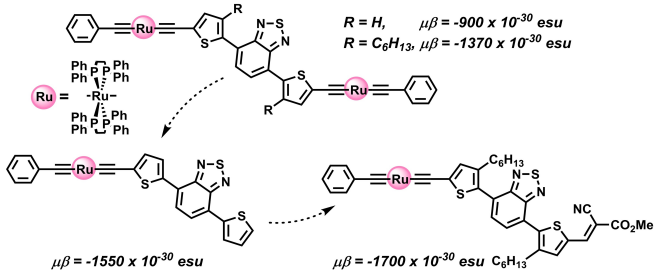

Scheme 2. Molecular designs endowed with high SHG signals. Adapted with permission from ref.[28] Copyrights 2014, Royal Society of Chemistry.

or pyridmidinium acceptor group (Scheme 3). The later leads to a very strong charge transfer character evidenced by the large bathochromic shift of the MLCT band down to 683 nm leading to the highest quadratic hyperpolarizability values reported so far for monometallic metal-alkynyl derivatives ($\mu\beta_{EFISH=}$14000 10^{-48} esu).

Quadratic hyperpolarizabilities of branched "Y-shaped" molecules were also investigated by Humphrey and co-workers.[30] Clearly, polarizing substituents ($-NO_2$) are mandatory to induce strong charge transfer (Ru→NO_2) and high HRS activity in this molecular series. Indeed, introduction of an electron withdrawing *nitro* group along the C_2 axis of the molecule results in $\beta_{HRS,\ 800}$ of 112 10^{-30} esu, and of 221 10^{-30} esu when nitro moieties located on the molecule's arms comprising the Ru centers. In the same spirit, further improvement of the quadratic hyperpolarizability was obtained with octupolar metallodendrimers.[1,27,31] First generation dendrimer containing up to three metal centers and where the metals were functionalized by Ph-NO_2 acetylide ligands displayed significant β ranging from 93 10^{-30} esu to 221 10^{-30} esu, greater than the sum of its linear components. Moreover, increasing the number of [Ru]C≡CPhNO_2 (2nd generation dendrimers) enhanced the β_{1064} value up to 1880 10^{-30} esu confirming the essential role of the strong Ru→NO_2 charge transfer and highlighting that the quadratic hyperpolarizability scales with the number of Ru centers.

Quadratic hyperpolarizability measurements were mainly performed in solution whereas actual frequency doubling device would necessitate working in solid state or with solid matrices. To that end, few groups reported SHG measurements in PMMA films.[28,31] De Angelis, Dragonetti and co-workers with their best candidate observed a promising, stable overtime SHG signal once the PMMA film was exposed to ambient conditions.[28] Fillaut and Katan[31] also investigated SHG properties of a monometallic compound in both PMMA and in a photocrosslinked acrylic matrix (Figure 5). They obtained a low but sizeable SHG signals once the electric field was shut down, though the signal intensity tend to decrease with time.

3rd and higher order NLO studies. There has been a great deal of research regarding the development of organic, organometallic and coordination derivatives displaying multiphoton absorption (MPA).[32] In particular, Ru acetylide derivatives exhibited outstanding MPA. This non-linear character has still to be related to the Ru d/π–π* charge transfer band, and the introduction of a PhNO_2 electron withdrawing moieties usually increased the 2PA cross-sections whatever the nature (dipolar, centrosymmetric, quadrupolar or octupolar) of the molecule as for 2nd order. The results were summarized in a recent review published by one of the main contributor to this field.[27f]

Interestingly, Paul and co-workers investigated the impact on the 2PA merit with a synergetic association of Ru centers with a porphyrine platform, a moiety known to provide MPA activities. The authors observed that the 2PA merit scales with the number of metal centers (Figure 6), σ_2 ranging from 7500 GM for a mono ruthenim association to 16 000 GM for a tetra-ruthenated specie.[33] Even larger 2PA cross-sections could be obtained using a dendrimer approach (Figure 7).[34] π-

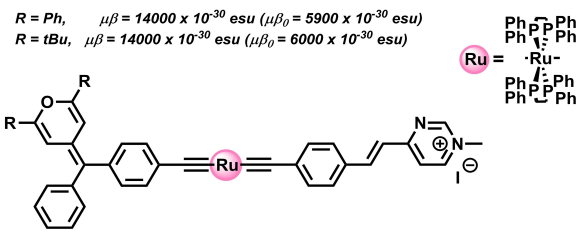

Scheme 3. Donor-Ru-Acceptor dipolar molecule developed by Gauthier and co-workers showing the highest μβ value for metal-alkynyl derivatives. Adapted with permission from ref.[29] Copyrights 2016, Royal Society of Chemistry

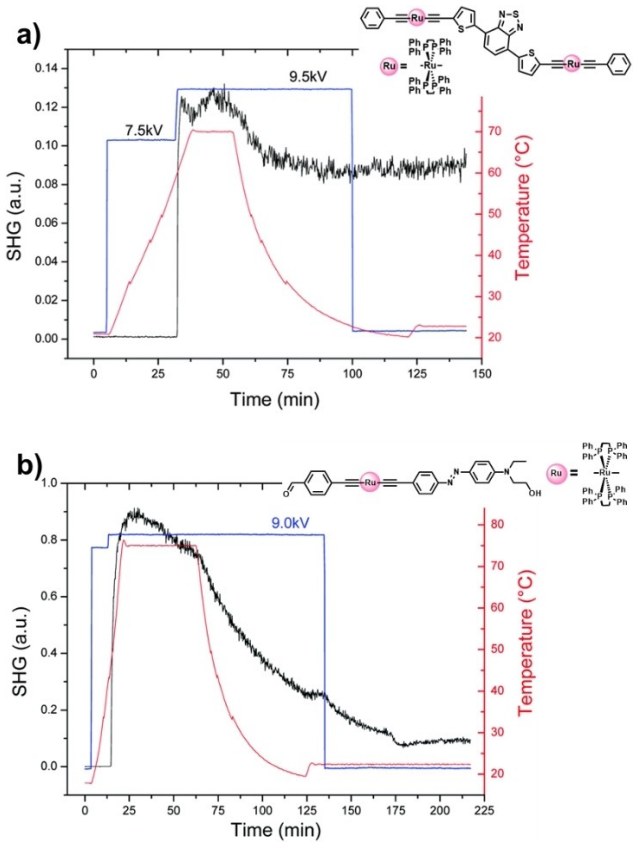

Figure 5. SHG experiments performed on acrylic films doped with bimetallic (a) and monometallic (b) derivatives. Adapted with permission from refs.[28,31] Copyright 2014, Royal Society of Chemistry.

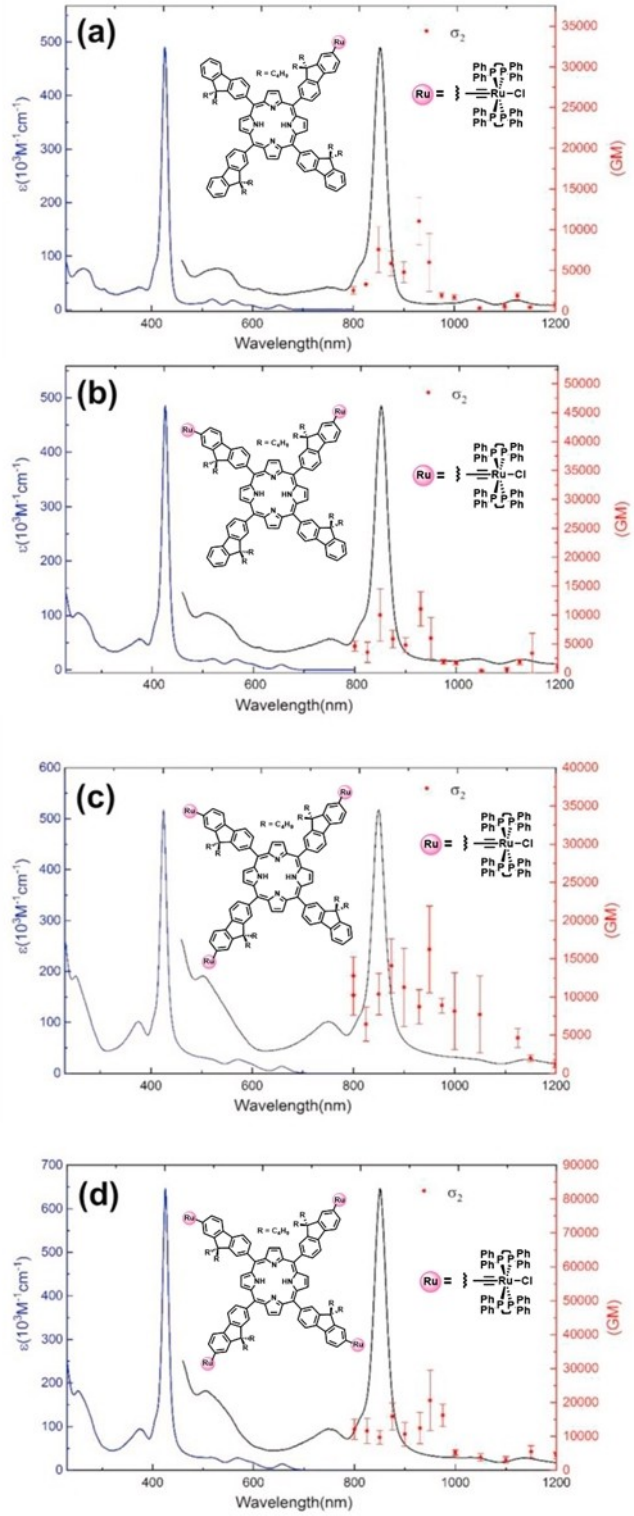

Figure 6. 2PA absorption cross-section plots (red line) for monometallic (a), bimetallic (b), trimetallic (c) and tetrametallic (d) compounds overlaid with the 1PA absorption spectra (blue line) and the same 1PA spectra plotted at twice the wavelength (black line). All compounds show a fair match between their 2PA cross-section spectra and their 1PA plotted at twice the wavelength. Adapted with permission from ref.[33] Copyright © 2021 Elsevier Ltd.

extension combined to increased number of Ru centers up to 45 metal centers has led to gigantic σ_2 of 50600 GM at 900 nm.

Moreover, the most intriguing property of these metallodendimers is their ability to absorb more than two photons simultaneously. In other words, these compounds also exhibited high 3PA, 4PA and 5PA cross-sections. Humphrey and coworkers clearly demonstrated that the 3–5PA cross-sections maxima corresponded closely to the appropriate multiples of

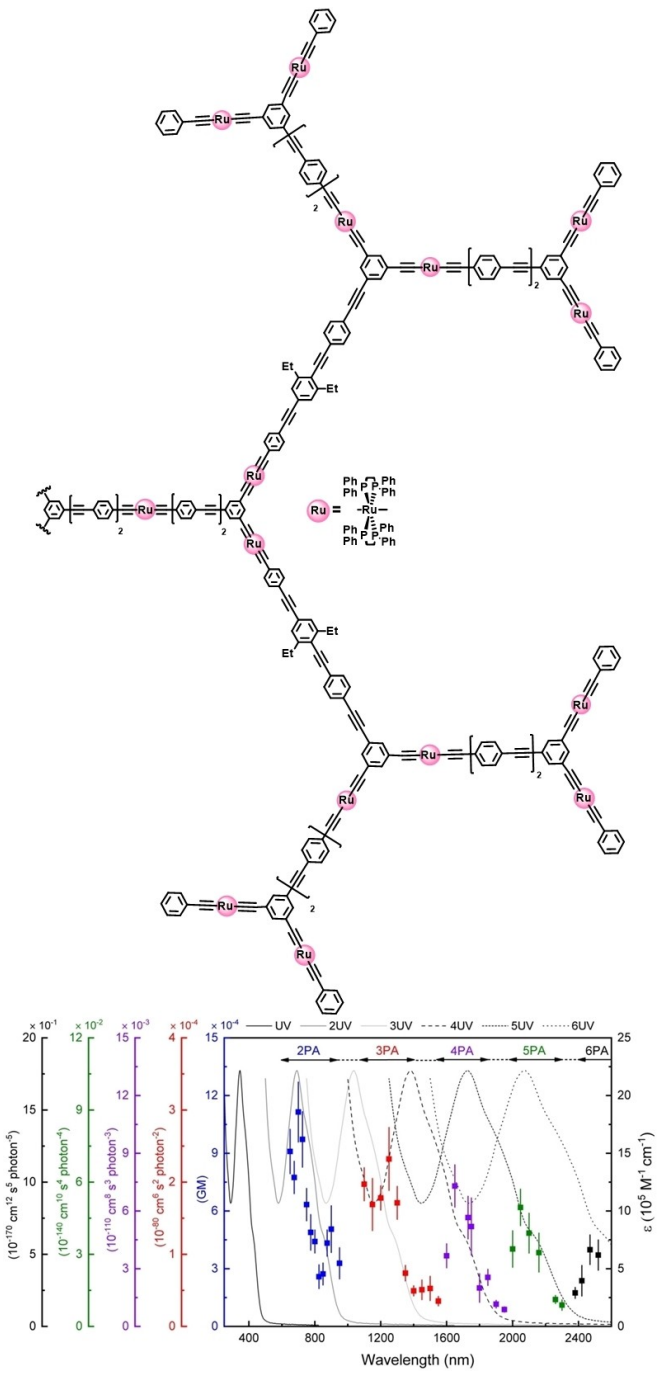

Figure 7. Third generation metallodendrimer comprising a total number of 45 metal centers displaying high 2PA cross-section at 900 nm. Adapted with permission from ref.[34] Copyright © 2022 The Authors.

the molecule low-energy MLCT band, highlighting again the essential role of Ru center in creating a strong charge transfer character. They could even measure a weak but sizeable 6PA cross-section $\sigma_6 = 53\ 10^{-170}\ cm^{12}\ s^5\ photon^{-5}$ at 2470 nm, a record. To rationalize the effect of dendrimer formation upon the improvement of 2PA cross-sections, the authors corrected the measured values by the number of effective electrons, a concept introduced by Kuzyk[35] and which takes into consideration the contribution of the π-system electrons. Overall, the authors observed a clear increase of the corrected 2PA cross-section yet without any linear effect.

In their latest study, Humphrey and co-workers replaced the central benzene core by a C_3 symmetric electron poor heptazine motif on the way to further increase the charge transfer character of the MLCT transition.[36] As a result, the compounds outperformed the previous molecules, displaying 100 times greater 2PA cross-sections compared to their benzene-centered parent. The four heptazine derivatives also presented sizeable 3PA (at 1600–1730 nm), 4PA (2100–2300 nm) with impressive cross-sections, surpassing the MPA-active in the NIR-III spectroscopic window reference compounds. Interestingly, the heptazine functionalized molecule featuring electron donor ($-NEt_2$) group located on the Ru arms better performed than its NO_2 containing parent. This is in clear contradiction to what was always observed by this research group, suggesting that the Ru functionalization has to be adapted depending on the electron poor/rich character of the dendrimer's central ring. This result also suggests that replacing benzene knots into the previous 3rd generation dendrimers (Figure 7) by heptazine moieties may positively affect the MPA activity of such kind of molecules.

3. Electro/Photo-Switchable Molecular Materials Containing Ru^{II} Alkynyl Derivatives

Recent researches have shown that the redox-active ruthenium acetylides can promote unique electro- or photo- switching of specific optical or magnetic properties when they are associated with *ad hoc* moieties.

3.1. Redox Switchable Magnetic Systems

Molecular magnetism is an attractive research area with respect to new materials that might be prepared, and many efforts have also been invested in the elucidation of the role, sign, and magnitude of exchange coupling of unpaired electrons. A question of particular interest was how the ruthenium moieties can act as a redox-controllable magnetic coupling units (MCU) between remote radicals, knowing that a bis-ethynyl-phenyl-nitronyl-nitroxide platinium complex displays a weak coupling between the two radicals ($0.1 < |J| < 1\ cm^{-1}$) through the non-redox active diamagnetic transition metal. As expected, with the help of EPR spectroscopy, It was demonstrated that the diamagnetic $[Ru(dppe)_2(-C{\equiv}C-R)_2]$ system sets up stronger magnetic couplings between two organic radicals R, i.e., two nitronyl nitroxide or two verdazyl units, of ca. −2 and −4 cm^{-1}, respectively.[37] Surprisingly, further oxidation of the ruthenium redox-active MCU, which introduces an additional spin unit on the carbon rich part, leads to the off-switching of this interaction. Further study of another ruthenium carbon-rich complex $[Ru(dppe)_2(-C{\equiv}C-bipyCu^{II}(hfac)_2)]$ (bipy = 2,2-bipyridin-5-yl) show that the neutral ruthenium system also sets up a magnetic coupling between two remote paramagnetic Cu^{II} units ($-4.8\ cm^{-1}$) via a spin polarized mechanism (Scheme 4).

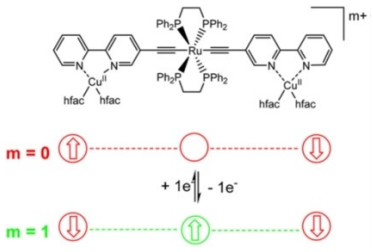

Scheme 4. The ruthenium system as a MCU. Reproduced with permission from ref.[37] Copyright © 2015, ACS.

Surprisingly, oxidation of the ruthenium MCU again leads to weaker magnetic interactions; the magnetic interaction is now largely dominated by the lower antiferromagnetic coupling between this spin carrier and the Cu^{II} end groups, which is an unusual phenomenon. This copper compound is a unique example of linear heterotrimetallic compounds with exceptionally long distances between the spin carriers (8.3 Å between adjacent Cu and Ru centers, 16.6 Å between external Cu centers), for which a complete rationalization of the magnetic interactions (DFT) could be made and compared in two different redox states.

Another combination of interest is the coupling of ruthenium acetylides with Single Molecule Magnets (SMM), which at low temperature behave as tiny magnets at the molecular scale. SMM have raised enormous interest in recent years especially with the use of a single anisotropic lanthanide ion. Therefore, with the attractive perspective of manipulating an individual magnetic molecule by means of an electrical (redox) potential, association of a highly anisotropic Dy(III) ion and a ruthenium-acetylide was achieved with trans-[PhC≡C-$(dppe)_2$RuC≡C–bipy($Dy^{III}$$(acetylacetonate)_3$)] (acetylacetonate$^-$ = tta$^-$ or hfac$^-$) (Figure 8).[38] An unexpected high resulting symmetry for the Dy(III) coordination site leads to an unusual SMM behavior with the presence of multiple relaxation mechanisms which can be activated/deactivated by an external field. After oxidation of the hfac adduct, at 2 K and with H_{dc} = 800 Oe, the relaxation is significantly slower (0.33 Hz vs. 12.4 Hz prior oxidation) in the entire investigated range of temperatures. This result evidences the switching of a pure 4f SIM into a 4f – 4d SMM, with enhanced dynamical properties due to either modification of the lanthanide crystal field or creation of an additional spin carrier upon oxidation delocalized on both the 4d ion(s) and the carbon-rich ligand(s), perturbating the 4f ion. Note that further *trans* functionalization of such systems offers an enhanced potential for increased functionality.

Overall, these few studies open up horizons toward versatile molecular magnetic devices tailored by an external redox stimulus, with precise molecular engineering, based on the Ru^{II}-acetylide moiety. To our knowledge, these two molecules represent unique redox switchable magnetic systems so far.

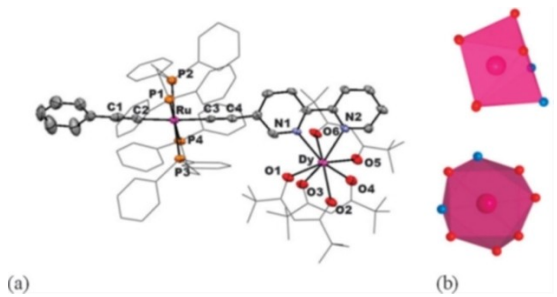

Figure 8. (a) Simplified view of the crystal structure of the tta complex, (b) Dy atom coordination sphere. Reproduced with permission from ref.[38b] Copyright 2014, ACS.

3.2. Ru^{II} Alkynyl Endowed with Photochromic Units

The ubiquitous diarylethene (DTE) is one of the most promising photochromic systems due to its high fatigue resistance.[39] It can be efficiently switched from a non-conjugated form to a conjugated form upon UV irradiation, and switched-back using visible light (Scheme 5). Therefore, this unit has been used for the photoregulation of various properties including sensing,[40] NLO,[41] magnetism,[42] molecular conductance,[43] redox behavior,[44] NIR absorption,[45] optical rotation,[46] super resolution imaging,[47] catalysis,[48] and so on.

However, multi-DTE systems with π extended conjugation often display partial photocyclization because of facile intramolecular energy transfer from the ring-open moiety to a ring-closed one that prevents further photocyclization. Interestingly when the $Ru(dppe)_2$ motif is inserted into a conjugated multi-DTE system, full closing with *distinct stepwise* ring closing is attained,[49] in contrast to Pt bis-alkynyl systems,[49d] In particular, Chen and collaborators demonstrated with an asymmetric complex (Figure 9), incorporating two different DTE units with well separated ring-closing absorption bands,[49c] stepwise photocyclization and selective photocycloreversion upon irradiation with appropriate wavelengths. This system affords four states (**oo**, **co**, **oc** and **cc**) not reachable with symmetrical complexes. The photochromic properties of the oxidized species were also investigated and show similar photochromic characteristics. To better elucidate the mechanism at stake, deep investigations of the molecule's photophysics should be undertaken. Overall, it appears that the Ru center balances the coupling between the two photochromic fragments, which therefore behave independently, a useful feature to construct multi-photochromic systems.

Importantly, efficient opening or closing of DTEs can also be reached electrochemically,[44,50,51a–b] in contrast to similar Pt or Fe

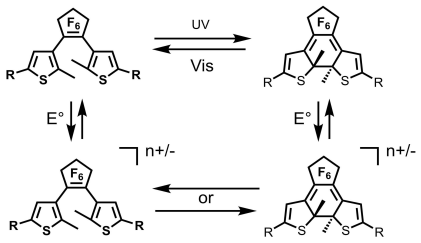

Scheme 5. Photochemical and electrochemical DTE switching.

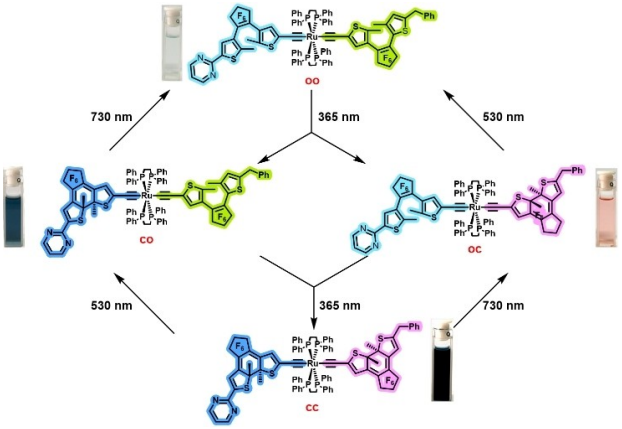

Figure 9. Multi-DTE ruthenium system from Chen and co-workers showing stepwise ring closing.

derivatives,[53] depending on the relative stabilities of the open and closed forms of the electrochemically produced species (Scheme 5). In particular, ring closure can be triggered electrochemically by oxidation of organic DTE unit, but it requires a relatively high potential (>1 V vs SCE).[44a,b] Attaching an organometallic unit to a DTE unit is an excellent strategy to modulate the electrochemical switching properties,[52] and to achieve multifunctional systems within a single component architecture. In that direction, we[44c,50,51] and others, with related Ru systems,[53] have shown that DTE association with a ruthenium carbon-rich system in a bimetallic assembly, such as in Figure 10, can afford photo-/electro- controllable molecular switches with an electrocyclization at remarkably low voltage (0.4–0.5 V vs SCE). The study also showed that slight modification of the *trans* carbon-rich ligands remote from the DTE unit modulates the spin density on the DTE unit upon oxidation and the ring closure kinetic, highlighting the remarkable influence of this ligand. The electrochemical cyclization was established to occur in the second oxidized state (EEC mechanism), whereas cyclization in the first oxidation state is the commonly accepted mechanism for organic units (ECE mechanism). The full or stepwise photo- or electro-closing of two *identical* photochromic DTE units in a related trimetallic molecule was also achieved with a combination of the optical and electrochemical and stimuli.[50] Interestingly, the Humprey's group reported on a NLO-active similar complex $Cl(dppe)_2Ru$-($C{\equiv}C$–C_6H_4–$C{\equiv}C$–DTE–$C{\equiv}C$–C_6H_4–$C{\equiv}C$)-*trans*-$RuCl(dppe)_2$]. The molecule displays effective modulation if its cubic NLO properties between six different states (neutral, oxidized, protonated). The authors also demonstrate that this compound displays no electrochromic behavior, probably due to weaker spin densities on the *adhoc* carbon atom for cyclization in the oxidized state, too remote from the ruthenium atoms.[54]

Others associations with photochromic spiropyrans have also been reported by Koustantonis (Scheme 6).[55] In particular, it was demonstrated that the introduction of a *trans*-[$RuCl(dppe)_2$] moiety into an alkyne-functionalised nitrospiropyran increases the lifetime of the merocyanine form by more than twenty-fold, compared to that formed from the parent ethynyl spiropyran, owing to a greater delocalization of charge with the ruthenium moiety.[55a] The same group recently developed a series of multifunctional bimetallic compounds where the spiropyran photochromic unit was flanked by the two metal centers (Scheme 6).[55b] However, in this configuration, the authors observed the complete vanishing of the photochromic activity.

They assigned this to a potential quenching of the photoprocess by a charge transfer mediated by the metal-acetylide fragment, or to the absence of NO_2 group in the 6-position of the spiropyran moiety which is known to provide high photochromic efficiencies.

3.3. Chiroptical Switches

Helicenes are molecules formed of *ortho*-fused aromatic rings that adopt a helical shape because of the steric hindrance between the terminal rings. They find applications as chiral molecular materials or asymmetric catalysts. Several types of helicene-based chiroptical switches have been developed, for which the switching process is mainly triggered by light, redox, or acid/base stimuli. We extended this concept to the dual redox and optical control thanks to ruthenium enantiopure complexes.[56] Complexes consisting of ruthenium-bis acetylides linked to helicene and DTE units were prepared and their strong

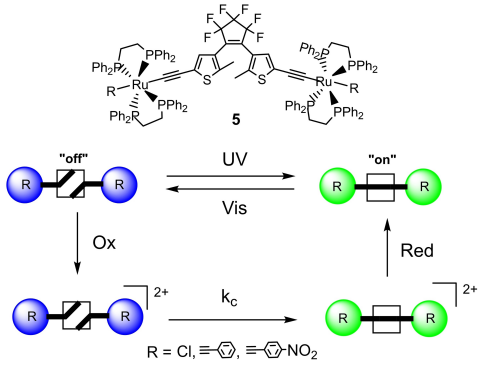

Figure 10. Photochromic DTE-ruthenium bimetallic assemblies also leading to low voltage electrochemical closing. Reproduced with permission from ref.[44c] Copyright 2014, ACS.

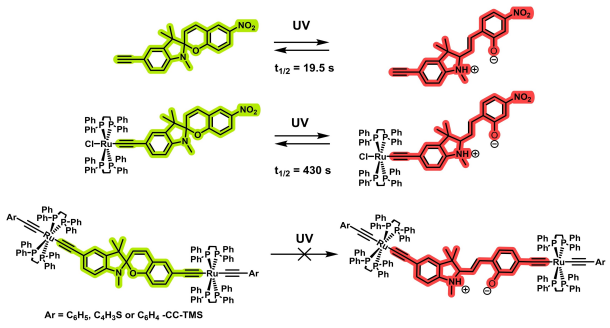

Scheme 6. (Top and middle) Introduction of a ruthenium moiety to an alkynyl functionalized spiropyran. (Bottom) Introducing two metal centers kills the spiropyran photochromic activity.

chiroptical responses provide tags that can be used for reading out the system, especially with electronic circular dichroism (Figure 11). The photochromic properties were studied, and further attractive electrochromic isomerization processes were also observed, i.e., a spontaneous reopening of $[\mathbf{1c}]^{\cdot+}$–$[\mathbf{1o}]^{\cdot+}$ (Figure 11, top) and the expected ring closure of $[\mathbf{2o}]^{2+}$–$[\mathbf{2c}]^{2+}$ similar to that described above (not represented). Due to strong chiroptical response, each redox or optical addressing can be monitored as illustrated in Figure 11 (middle) for the electrochemical oxidation of [**1o**].

Hence, these chiral complexes correspond to new types of chiroptical switches, triggered by light and/or redox stimuli, and that could be described as either "NOR" or "OR" logic gates.

3.4. Luminescent Switches

Molecular luminescent switches form a unique and fascinating class of compounds which luminescence response can be toggled with chemical or physical stimuli.[57] In the field of fluorescent materials, more and more attention is devoted to emitters in the near infrared (NIR) region, for several reasons,[58] such as the high transparency of biological tissues[59] that renders *in vivo* sensing and imaging more accessible with NIR emissive probes[58c,60] or, in the field of material science, reduced energy consumption, better photostability, or specific signatures difficult or impossible to detect with the naked eye. In this context, one can foresee the importance of NIR emission *remote control* in molecular systems for applications such as high resolution imaging or to provide security tag with more advanced encryption methods.[61]

Of particular interest are the NIR emitting lanthanides (Nd^{III}, Yb^{III} or Er^{III}), which feature narrow, sharp and intense emission lines.[62] Therefore, our group and others became very interested in the design of lanthanide complexes with controllable dynamic NIR emission. With the associations between Yb^{III}, Nd^{III} ions and a redox active ruthenium acetylide complexes bearing a bipyridine chelating unit, we built original d-f heterometallic complexes (Figure 12).[63] Efficient sensitization in the visible range of both NIR emitters was achieved with the ruthenium-acetylide antenna, through the MLCT at $\lambda_{max} = 460$ nm. For example, upon excitation, the characteristic line shape emission of ytterbium ($^2F_{5/2} \rightarrow {}^2F_{7/2}$) was observed (Figure 12). The luminescence of these complexes was modulated with a redox agent[63] and electrochemically.[64] In the latter case, Figure 12 shows the luminescence response obtained upon oxidation where the emission intensity decreases of ca. 100% and further recovered to 87% of the original intensity. The process can be rationalized either by the oxidation of the ruthenium acetylide moieties preventing any sensitization by an electron transfer mechanism, or by the apparition of new excited states at *c.a.* 1060 nm due to multiple transitions from HOMO-n to the SOMO resulting from the depopulation of the HOMO d_π/π orbital. These low-lying excited states can either prohibit the Yb^{III} sensitization and/or afford a preferential non-radiative back-energy transfer pathway from the Yb^{III} excited state.

In a further work, we accomplished the double photochemical and electrochemical control of Yb^{III} luminescence (Figure 13).[65] The new system takes benefit of the photostimulation of three DTE units coordinated to the Yb^{III} center by

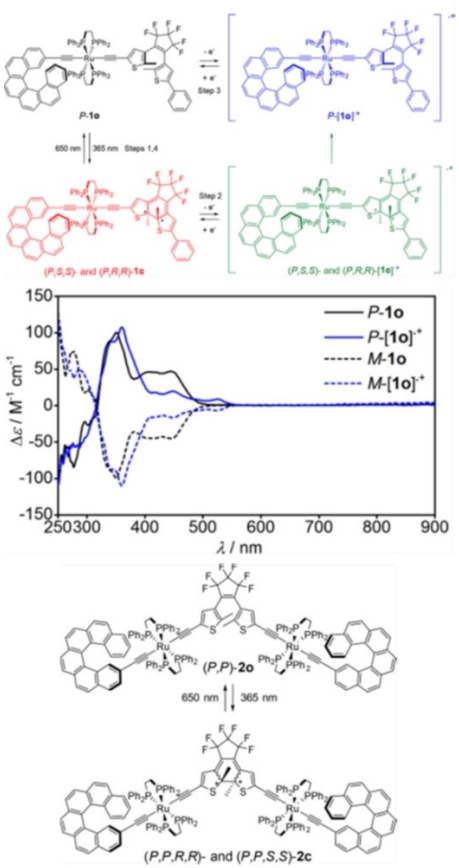

Figure 11. (Top) Photochromic and electrochromic steps of 1o. (Middle) ECD spectra of the open-state P- and M-1o and of the open oxidized state P- and M-$[1o]^{\cdot+}$. (Bottom) Photochromic Switching between 2o and 2c. Reproduced with permission from ref.[55] Copyright 2018, ACS.

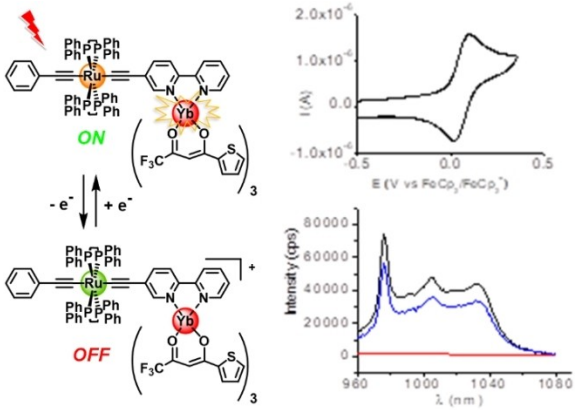

Figure 12. (left) Luminescent redox-switchable complex (right) Redox process and CV trace of the Ru–Yb complex (CH_2Cl_2, 0.2 M Bu_4NPF_6, v = 100 mV s−1), and monitoring of the emission spectra ($\lambda_{ex} = 440$ nm) upon its first oxidation in an OTTLE cell (CH_2Cl_2, 0.2 M Bu_4NPF_6): Initial emission spectrum in CH_2Cl_2 (black), after oxidation at 0.8 V vs. Fc^+/Fc (red), and after reduction at 0 V (blue). Reproduced with permission. Copyright 2014, ref.[63] Copyright © 2011, American Chemical Society, ACS.

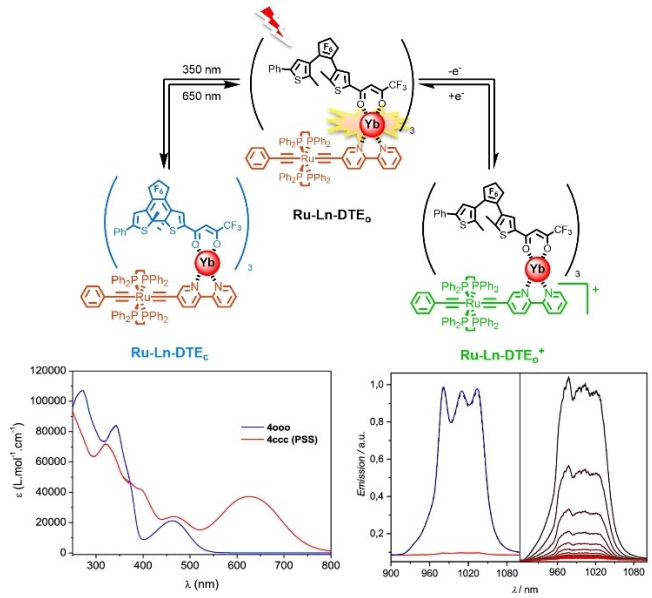

Figure 13. (Up) chemical formula of Ru–Yb-DTE in its different forms. (bottom) Initial absorption (emission) spectrum of Ru–Yb-DTEo in CH_2Cl_2 (blue), after UV irradiation (λ_{irr} = 350 nm, red), and then bleaching (λ_{irr} = 650 nm, dashed) with λ_{ex} = 450 nm. Emission decay upon UV irradiation. Each spectrum is recorded with a 1 s time lapse.). Reproduced with permission from ref.[65] Copyright 2019, ACS.

a β-diketonate moiety and of the above mentioned ruthenium redox switching. The MLCT transition (λ_{max} = 450 nm) can still be used to trigger ytterbium response at λ_{max} = 980 nm. Further experiments showed (i) the vanishing (to 1.4% of initial maximum intensity) of the luminescence signal after UV treatment (λ_{irr} = 350 nm) and DTE closures at the PSS, and (ii) a total recovery of the emission signal up to its initial intensity after visible treatment (λ_{irr} = 650 nm) with reopening of the DTE photochromic components. We then established that excitation in the MLCT band offers an effective non-destructive readout of the system state. A dynamic photoswitching response was demonstrated: when excitation was performed at the photocyclization wavelength (λ_{irr} = 350 nm) with the DTE ligands or the bipyridine unit as sensitizers, a fast decrease of the NIR emission was observed. The hypothesis of a closed DTE triplet excited state lying at lower energy than that of the $^2F_{5/2}$ excited state of the Yb^{III} ion (10 200 cm^{-1}) is the most likely quenching mechanism.[39a] Electrochemical methods coupled to fluorescence spectroscopy was further applied to demonstrate redox switching. Oxidation causes a drastic drop in the signal intensity down to 12% of its initial value, which can be nearly fully restored (93%) upon electroreduction. We also designed a related complex with one DTE ligand attached on the trans acetylide ligand with respect to the Ln centers bearing simple tta-ligands.[66] This new design features an efficient closing reaction leading to the quenching of Yb^{III} emission that can be triggered as expected by UV light (350 nm) but also by lower energy blue light (450 nm) as the DTE is now conjugated to the ruthenium center. This results in an energy transfer to the DTE unit and further ring closure, also preventing non-destructive readout. This highlights the importance of a precise engineering and the powerful association of a Ru alkynyl center and DTE moiety. The next step towards applications will then consist in the optimization of the observed behaviors in terms of brightness of the molecular probe in its ON state, and we foresee many improvements and developments of original systems.

Owing to their rich optical and electrochemical properties, porphyrins are also appealing units to incorporate into multicomponent systems to build switchable systems. Porphyrins have been extensively used as light harvesting antennas and, therefore, photoinduced energy transfer from zinc porphyrin (ZnP) to free base porphyrin (P2H) is a well-established process. Hence, the development of a redox switch in which the efficiency of the photoinduced energy transfer between the two porphyrins can be controlled via the oxidation state of an electroactive bridge is appealing. The possibility of triggering the fluorescence signal of a dyad and a triad through the oxidation of a ruthenium acetylide bridge was then investigated.[67] The Ru-ZnP dyad exhibits a redox driven quenching of the fluorescence, since oxidation of the nearby ruthenium complex is accompanied by a modulation of the fluorescence intensity of ZnP. The most probable quenching process is the electron transfer from the singlet excited state of ZnP to the oxidized diethynyl ruthenium unit. In the ZnP–Ru-P2H triad, a different behavior is observed, both porphyrins' fluorescence are highly quenched independently of the redox state of the ruthenium bridge owing to an efficient photoinduced charge transfer within the ruthenium complex. The modulation of the energy transfer from ZnP* to an energy acceptor fluorophore via the oxidation state of the ruthenium complex can be, however, still envisioned in the future by using another spacer to modulate the rate of charge transfer reactions or by choosing an energy acceptor fluorophore. The former behavior was further confirmed by Paul and coworkers with two related dyads, containing tris- and tetrakis-meso-fluorenyl-substituted porphyrin and ethynylruthenium units, with a decrease in intensity during a first oxidation and further decrease upon a second oxidation.[68] With the aid of hybrid-DFT computations, they proposed a rationale, including for apparently contrasting observations reported by Akita for other porphyrins appended with closely related redox-active Cp*M-(dppe) (M = Ru, Fe) acetylides displaying fluorescence increase upon oxidation.[68] Overall, these studies are guides for molecular engineering of new redox driven switchable photoluminescent systems with improved performances.

4. Charge Storage or Transport Properties of Ru(II) Acetylide Compounds

4.1. Ru Alkynyl Compounds and Electron Transfer Exchange at Self-Assembled Monolayers for Memory Applications

Surface functionalization through self-assembled monolayers (SAMs) onto metallic substrates constitutes a powerful approach to design functional materials for use as data storage and transfer in integrated devices.[69,70] Ferrocene is often used

as a reference redox center for its low oxidation potential, fast electron transfer and robustness, compatible with SAMs stability. The ruthenium complexes have been first identified as possible candidates for charge storage for Quantum Cell Automata (QCA) with a cationic *dppm* analogue Ru(dppm)$_2$(C≡CFc)(NCCH$_2$CH$_2$NH$_2$)][PF$_6$] connected to doped Si (111) surface (Scheme 7).[71] Oxidation of the complex, formally of the ferrocene unit, generates a stable biased Fe^{III}–Ru^{II} mixed-valence complex on the surface. Capping with an Hg electrode and analysis of the differential capacitance of oxidized and unoxidized bound complexes show that electron exchange occurs from the Fe^{III}–Ru^{II} configuration to the Fe^{II}–Ru^{III} configuration with the electrical field.

In their work, Bruno and co-workers further immobilized the dppe system on silicon via hydrosylilation (Scheme 8).[72] They nicely demonstrated that a dinuclear Fe^{II}/Ru^{II} compound exhibited stepwise (Fe then Ru) electron transfer between the Si surface and the metal centers, however with a moderate rate constants of ca. 300 s^{-1} for the Ru oxidation. Later, they reported an in-depth investigation on a family of heterometallic Ferrocene – Ru^{II} alkynyl molecules, still grafted on Si surfaces, showing that apparent charge-transfer rate constants for the ferrocene system from the molecules to the surface were considerably higher than those reported at that time on silicon-bound system, but the ruthenium oxidations lead to instability.

In order to broaden the scope of Ruthenium complexes and their potential applications, we built new series of ruthenium carbon-rich complexes (Figure 14) for further formation of SAMs on gold surfaces[73] with the ubiquitous thiol anchoring group, as well as with other dithiocarboxylic acid or isocyanide grafting units.[74] Saturated aliphatic short groups –CH_2– and –O–$(CH_2)_6$– were also inserted between the complex and the thiol

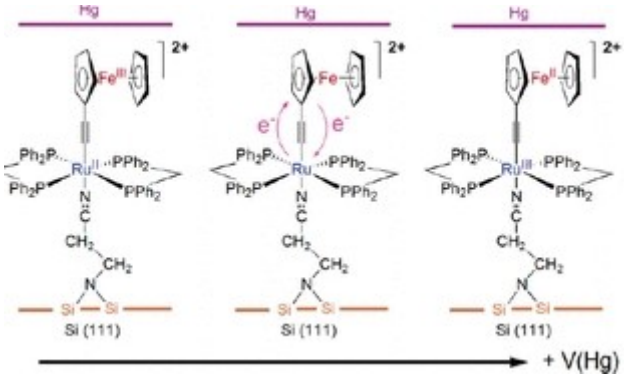

Scheme 7. Schematic representation of the experiment showing the mixed-valence complex as a function of the voltage imposed across a Hg and Si plates. Reproduced with permission from ref.[71] Copyright 2003, ACS.

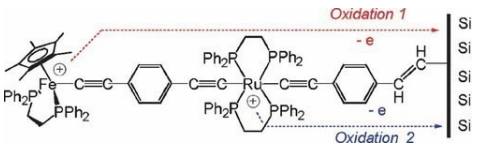

Scheme 8. Iron/ruthenium system by Paul and Fabre immobilized on silicon. Reproduced with permission from ref.[72] Copyright 2008, Wiley.

anchoring group, allowing a structural tuning which might have a significant impact on the quality of the SAMs and on the electronic coupling. Well-resolved oxidation wave were observed for all surfaces with $E^0 = 0.3$–0.5 V/SCE and fast electron transfer kinetics ($\approx 10^4$ s^{-1}) featuring no significant differences between all complexes. The values compare well with the fastest redox systems like ferrocenes (10^3–10^6 s^{-1}).[75]

Thus, the nature of the bridging and anchoring units has hardly any effect on the charge transfer rate constants in contrast to what is observed in charge transport measurements with molecular junctions (*vide infra*). The rate-limiting step for the electron transfer process in the monolayer is rather due to effects at the interface between the monolayer and the solvent/electrolyte.[76]

Interestingly, SAMs onto gold surfaces previously reported with polyferrocenyl centers may display ultrafast kinetics (10^6–10^7 s^{-1}) but with the observation of only one (bi-electronic) electrochemical process.[75a] Separated oxidation waves are sometimes observed but with an electron transfer rate constants 3 orders of magnitude smaller.[75b] Therefore, the construction of efficient electroactive surfaces for charge-storage medium is a challenging aspect requiring molecular systems which exhibit multiple oxidation states accessible at low potentials and fast electron-transfer rates (10^4–10^6 s^{-1}). To date mainly porphyrins-based architectures appear interesting,[77] along with one ruthenium cluster.[78]

Thus, owing to the excellent electronic delocalization within the carbon-rich path of ruthenium systems, four series of molecular wires consisting in mono-, bi-, and tri-metallic ruthenium(II) bis(σ-arylacetylide) organometallics were designed for SAMs formations (Figure 15).[79] High speed cyclic voltammetry studies evidenced again low oxidation potentials (0.2–0.7 V/SCE), even lower than those exhibited by porphyrin systems.[77] Remarkably, the Ru molecular wires exhibited discrete oxidation states that correlate with the number of connected ruthenium centers. In the polymetallic compounds, the $E^{\circ\prime}$ values for the first (for di-and tri-ruthenium complexes) and second (for tri-ruthenium complexes) oxidation processes are always lower than that observed for the corresponding mono-metallic analogues, reflecting a gain in stabilization for the oxidized species as the molecular lengths increase. Fast charge transfer kinetics were found with apparent rate constants still in the order of 10^4 s^{-1} that compare well with those of the porphyrin-containing SAMs.[77] Note that, here again, the variation of the anchoring groups and/or the bridging units has almost no influence on the electron transfer dynamics. Overall, those bis(σ-arylacetylide) complexes are powerful building blocks for designing molecular wires exhibiting key properties as charge-storage medium for multibit devices (up to 3 different oxidation events, hence 4 oxidation states) with low power consumption.

Finally, to be fully exploited in applications ruthenium complexes/DTE combinations were immobilized at an interface, knowing that a key issue being the effect of surface confinement on the photochromic switching function, whereas the redox switching is hardly affected. This might be due to excited states quenching, electronic relaxation effect or steric hindrance deriving from the lack of free space.[80] In this context, two DTE

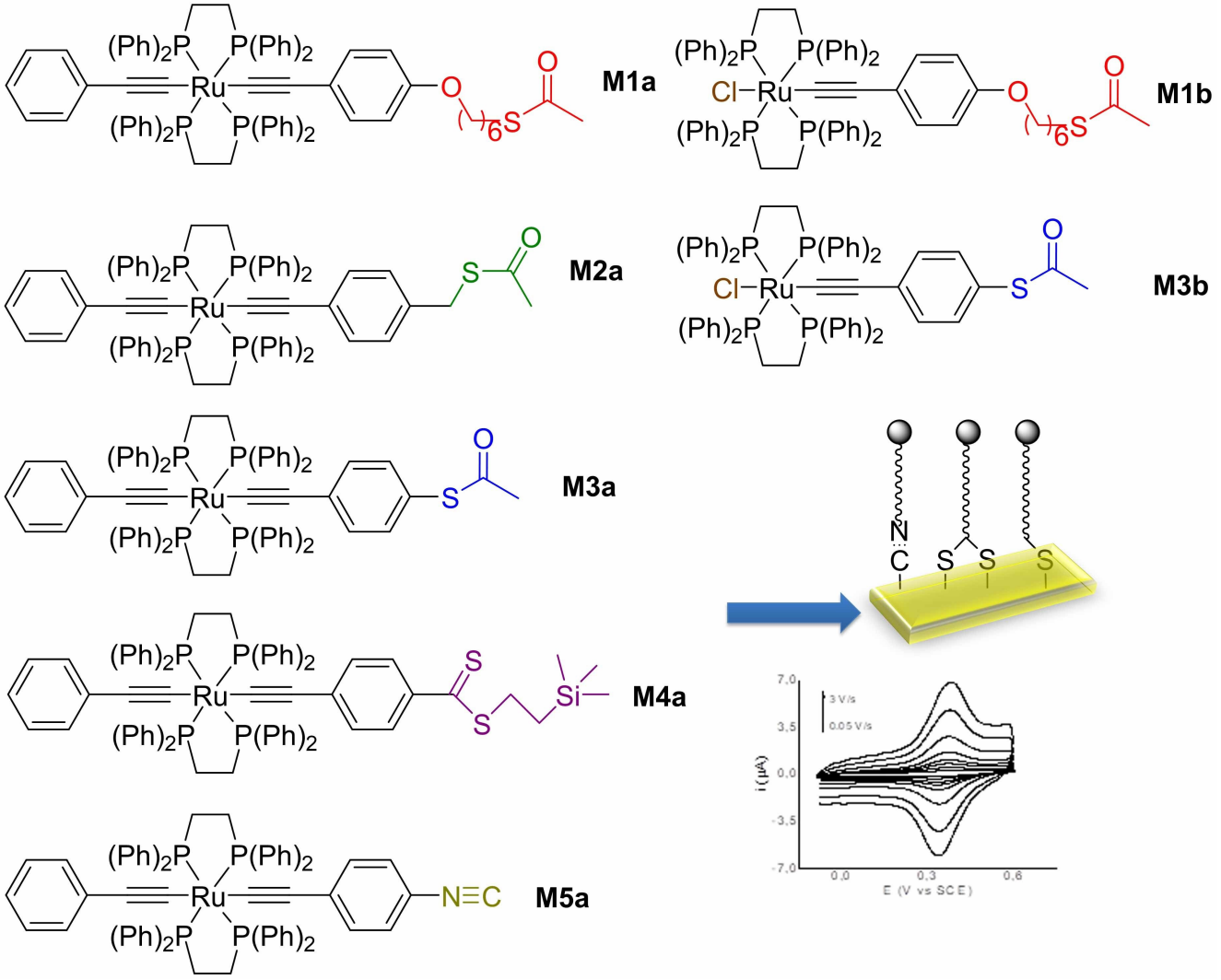

Figure 14. Molecular structures of the studied organometallic complexes (top). Cyclic voltammetry in CH_2Cl_2 (0.2 M Bu_4NPF_6) of gold electrode modified with a single components SAM of **M1a** onto an electrode (bottom). Reprinted with permission from ref.[73] Copyright 2015, ACS.

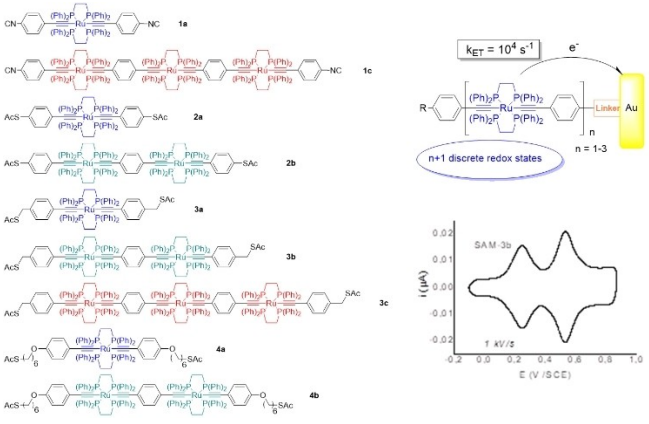

Figure 15. Molecular structures of the investigated polymetallic complexes (left). Scheme of the multiredox systems on surfaces, CVs of SAMs in CH_2Cl_2 (0.2 M NBu_4PF_6) of **3b** (right). SAMs were prepared onto gold ultramicroelectrodes Reproduced from ref.[79a] Copyright © 2015 WILEY-VCH Verlag GmbH & Co. KGaA, Weinheim.

carbon-rich ruthenium complexes with a hexylthiol unit were incorporated in SAMs on gold surfaces (Figure 15).[81] SAMs incorporating the monometallic molecule showed a reversible one-electron oxidation shifted towards less positive potentials upon photochemical ring closure (from $E^\circ = 0.43$ V–$E^\circ = 0.39$ V vs SCE). In sharp contrast, electrochemical switching of the bimetallic one is detected upon oxidation with (i) a signal at ca. 0.5 V corresponding to two very close monoelectronic systems, and (ii) subsequent cycling between −0.2 and 0.8 V at low scan rates that leads to the appearance of two reversible well-separated redox systems at lower potential characteristic of electrochemical-triggered ring closure of the DTE unit (*vide infra*). If the potential cycling is performed at high scan rates (> 5 $V s^{-1}$), the electrochemical switching does not occur because the electrochemically-triggered isomerization process is a slower process than CV cycling giving a "non-destructive" read out at high scan-rates (Figure 16). Photochemical isomerization was also successfully carried out for both compounds by irradiating the SAMs at 350 nm and 750 nm. Thus, these new SAMs exhibit

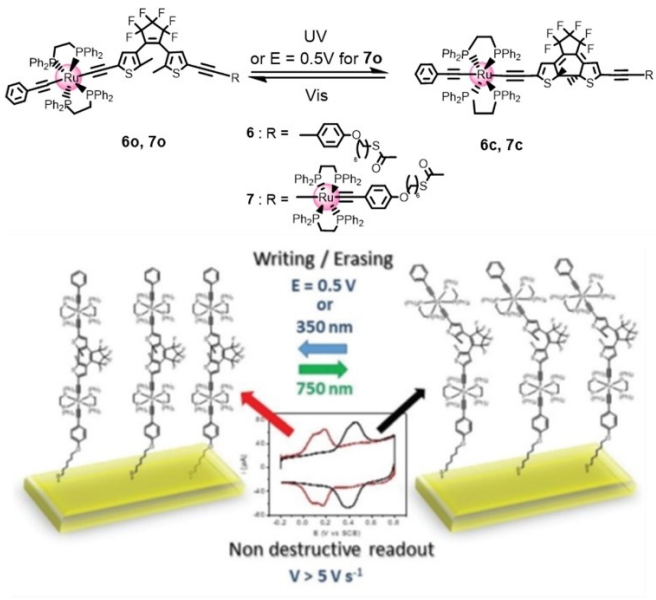

Figure 16. Cyclic voltammograms in CH_2Cl_2 containing NBu_4PF_6 of single-component SAMs on a gold disk electrode (ø 1.6 mm). SAM of **7o** (black line) and **7c** (red line), scan rate is 100 V s^{-1}. SAM of **7c** is obtained after cycling of SAM of **7o** with 5 repetitive cycles between −0.2 and 0.8 V at 10 mV s^{-1}. Reproduced from ref.[81] Copyright © 2017 Wiley-VCH Verlag GmbH & Co. KGaA, Weinheim.

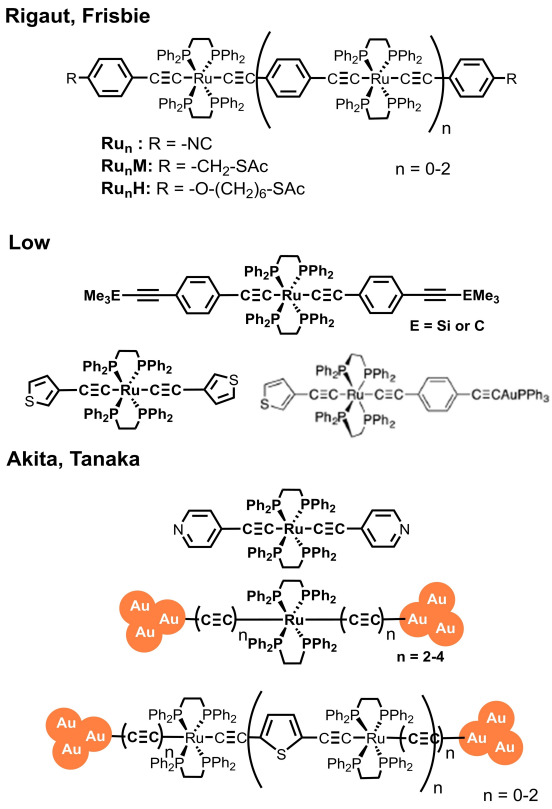

Scheme 9. Molecular structures of ruthenium wires.

read, write, and-erase functions, and can act as data storage interface along with an access to different oxidation states. They would allow for the implementation of more complex logic operations than in binary logic gates.

4.2. Ruthenium Organometallics in Molecular Junctions

Single molecules as active elements have been considered as potential building blocks for future nanoelectronic systems because of their advantages on cost, scalability, component density, and power consumption.[82] In addition, if the devices can be controllable with an external stimulus by choosing the appropriate chemical design, this technology should allow infinite possibilities for further developments (*vide infra*). Concerning the pure conductivity feature, rigid rod like π-conjugated oligo(phenyleneethynylene) (OPE) derivatives have emerged as benchmark molecules for studying charge transport in molecular junctions.[82f,g,83] Following the seminal example with Pt from Mayor and collaborator showing low conductance because of a limited d/π mixing,[84] several groups (Scheme 9) participated to further studies by probing the electrical conductivity of metal containing OPE derivatives with direct carbon rich metal σ-bonds.[3b,85–90] These compounds display attractive characteristics over organic OPEs with their linear structure, low oxidation potential and extensive mixing of the metal-based orbitals with both the supporting and bridging ligands, expected to provide a lower dependence of the charge transport on molecular length.

In 2007, in collaboration with Dan Frisbie, we reported the first electrical behavior of a series of redox-active metal acetylide conjugated molecular wires as a function of temperature and molecular length,[85d] using conducting probe atomic force microscopy (CP-AFM) and crossed-wire junctions. The wires endcapped with isocyanide (**Run**) surface linking groups consist of covalently coupled ruthenium(II) bis(σ-arylacetylide) complexes with length ranging from 2.4–4.9 nm (Scheme 9). A very weak dependence of the wire resistance with molecular length was found, consistent with a high degree of electronic communication along the molecular backbone (an attenuator factor $\beta = 0.9\ nm^{-1}$ is found whereas OPEs lead to attenuation factors of c.a. 2–6 nm^{-1}). Low temperature experiments (5 K) suggests coulomb blockade-like behavior for **Ru3**, whereas direct tunneling apparently occurs for the two other ones. Overall, these first results demonstrated the connection between charge transport mechanism and molecular length in molecular junctions. Further studies on the related complexes **RunH** and **RunM**, revealed that both series of molecular wires also exhibited very weak length dependence of the resistance ($\beta = 1.02\ nm^{-1}$ for **RunM** and 1.64 nm^{-1} for **RunH**). Importantly, further analysis of I–V characteristics with the temperature-dependent conduction measurements confirms that the charge transport in **RunM** and **Ru1H** junctions was direct tunneling, but in **RunH** (n = 2, 3) junctions the mechanism was thermally activated hopping.[85c] As expected the long insulating chains favor the hopping process. In the meantime, Wang and collaborators directly compared trans-Ru(dppe)$_2$(C≡CC_6H_4–SAc)$_2$ with the well-studied oligo(1,4-phenylene ethynylene) and

found higher conductivity for the former, ascribed to a lower band gap between its HOMO and the gold Fermi level.[82h]

Low and collaborators further reported that single molecule conductance of a ruthenium–acetylide wire (Scheme 9) with trimethylsilyl (TMS) terminal anchor showed a conductance peak greater than that of the corresponding phenylene ethynylene wire, while no peak was observed for the tert-butyl derivative (Scheme 9).[85g] Analogues with thiophene linking groups were also reported for comparison to Pt analogues showing here unexpectedly similar conductance values.[85f] Also, Akita and co-workers reported single molecule conductance (STM-BJ) of ruthenium fragments having pyridines as anchor groups and displaying higher conductance than that of molecular wire without the ruthenium fragments and of the same order as the thiol analogues.[86]

Importantly, more recently, Akita and Tanaka reported insertion of a Ru-$(dppe)_2$ fragment into polyynes to provide new metallapolyynes (Scheme 9), that improves conductance performance and hinders cross-linking owing to the bulky fragment. Indeed, $–(C{\equiv}C)_n–Ru(dppe)–(C{\equiv}C)_n$ - metallapolyynes are highly conductive ($10^{-3}–10^{-2}$ G_0; n = 2–4), even better than parent organic polyyne systems and feature a low attenuation factor similar to our previous findings (0.25 $Å^{-1}$) with a low contact resistance, thanks to the direct C–Au bonds to gold electrodes.[87] They also compared mono, bi and trimetallic compounds with this contact that display very small attenuation factors (0.07 $Å^{-1}$) due to the conjugation, the metal/metal interactions and the HOMO level lying close to the fermi level.[88] Note that Chen and co-workers arrived to similar conclusion for the attenuation factor with other monometalic oligoynil terminated complexes featuring phenyl methyl-thiols functions.[88]

Several other investigations were reported by Low,[80,85f], Loertscher,[85b] and Akita,[89] with various structural variations to fine tune the properties and to understand the property/structure relationships, including theoretical calculations, and also to compare them to other metal fragments. All the results are summarized in detailed reviews[85k,l] confirming that the conductance of organometallic junctions is superior to that of parent organic junctions, especially in the long distance range, and with rationalization of many factors such as linker, anchor group, molecular length, metal fragment, measurement method and conditions. All these studies point out that carbon-rich organometallic systems are suitable for the energy alignment brought about by the contribution of the metal d-electrons orbitals higher in energy. This leads to a higher HOMO and a better energy alignment occurs between with the electrode fermi levels essential for high conductance.

Interestingly, their promising electrical behavior also encouraged Low and collaborators to study the Thermally Induced Decomposition of an Organometallic Compound (TIDOC) method with trans-Ru-$(C{\equiv}C–3–C_4H_3S)(C{\equiv}C–1,4–C_6H_4C{\equiv}CAuPPh_3)(dppe)_2$ (Scheme 9) to form well-ordered, densely packed self-assembled monolayers on gold and silver substrates, contacted through the sulfur atoms of the thiophenyl groups for applications. Upon mild thermal treatment (150–200 °C) the gold moiety decomposes to liberate PPh_3 and form quite uniform disc-shaped gold nanoparticles on top of the organometallic monolayer to provide I–V curves characteristic of through-molecule conductance.[90]

Overall, those organometallics provides helpful insight for design of molecular electronics, not only for wires but also for more complex logic-task, as we show in the next section, and for another important property: thermoelectricity. Indeed, in the domain of molecular thermoelectrics at the nanoscale, which focuses on the Seebeck effect in molecular junctions, organic molecules usually exhibit a low or moderate efficiency due to their large HOMO – LUMO gap. Thermoelectric properties of molecular junctions incorporating organometallic complexes are thus of prime interest over organic molecules as first suggested by Low and co-workers with mononuclear ruthenium/platinium complexes with phosphite/phosphine ligands displaying interesting positive power factors of few μV/K.[91a]

More recently, Tanaka and Yoon reported multinuclear Ru$(dppe)_2$ complexes with aromatic bridging ligands and thioether anchors for thermoelectric investigations in eutectic Ga – In (EGaIn) junctions (Figure 17).[91] The Seebeck coefficient (S), ie. the thermopower, of the metal alkynyl complexes is varied by structural tuning of the complexes with metal nuclearity and substituents. Mononuclear complex **Ru_1** exhibited a S value of of 27 μV/K. The Seebeck coefficient increased to 62 μV/K for dinuclear complex **Ru_2H** and to 73 μV/K for trinuclear complex **Ru_3**. These outstanding values are significantly higher than those of oligophenylenes (SPh_m where m = 1, 2, 3; S = 8–13 μV/K) and are ascribed to the high proximity of the HOMO energy level to the Fermi level. Note that the positive sign of the S values confirms that the Seebeck effect is governed by HOMO rather than LUMO and hole tunneling. Thus, as expected, the thermopower decreased from 62–35 μV/K upon replacement of H atoms with electron-withdrawing (CF_3) groups on aromatic rings.

Overall, the possibility of achieving such high Seebeck coefficients opens a path to nanoscale devices for efficient energy management, including thermoregulation and heat-to-electricity conversion, as discussed in a very recent review.[92]

Finally, in this section, we wish to mention the use of Ru complexes for its topology to build tentative nanocars to be powered by an imaging tool, such as scanning tunneling microscopy (STM) (Figure 18).[93] Indeed, the octahedral ruthenium(II) complexes appeared to be suitable to serve as wheels, since the low rotation barrier around the alkyne bond

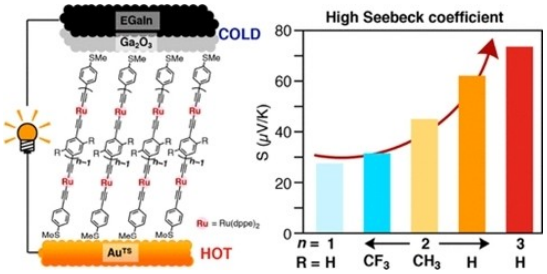

Figure 17. Illustration of the structure of the molecular junctions and of Seebeck coefficients. Reproduced from ref.[91] Copyright 2022, ACS.

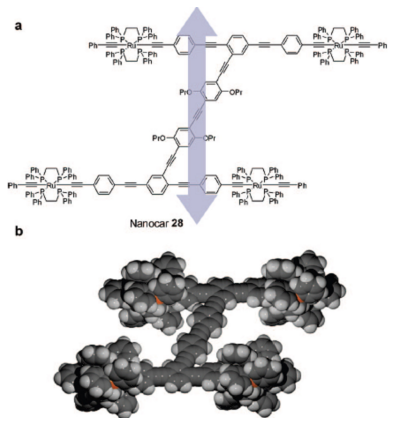

Figure 18. Nanocar with ruthenium wheels and their CPK model geometry optimized with SPARTAN. The arrows indicate direction of motion on surfaces. Reproduced from ref.[93] Copyright 2009, with permission from Elsevier

would allow a free rotation, while the bulky phosphine ligands might act as a tire to interact with metallic surfaces with good physisorption on metallic surfaces. With an overall wheel size of ~1.2 nm, the wheels should be clearly imaged by STM.

4.3. Ruthenium Organometallics for Switching Nanodevices

In order to exploit advanced nanodevices with promising applications, integration of photo-switchable molecules, such as dithienylethylene, stilbenes and azobenzenes, into nanodevices is receiving increasing attention.[94] Thus, the use of photochrome-coupled metal complexes,[95] appears to be attractive to produce original single molecule behaviors. An innovative step in that direction was to change the role the DTE photochromic unit from a simple photo-responsive unit in a molecular junction to a multifunctional one by realizing an additional redox triggered commutation in a junction with the use of the bimetallic DTE ruthenium acetylide complex (*vide supra*). Such an association of several stimuli to modify the conductivity of molecular junction in a single device to reach multi-functionality was indeed a pending challenge. In collaboration with Xiaodong Chen (NTU, Singapore), we tackled this issue by constructing new bimetallic and trimetallic compounds modified with thiol linkers, that we incorporated in nanogap device (Figure 19).[79b,96] The nanogap devices were further incorporated in a fluidic cell to achieve an electrochemical environment for device modulation, as shown in Figure 19.

The I–V curves of nanogap devices functionalized with the closed form of the bimetallic compound exhibited light-triggered switching, after the device was successively irradiated with visible light (700 nm) and UV light (365 nm). The switching in conductivity is explained by a weak delocalization in the photochromic part added to the polarization of the HOMO level of the open form. Importantly, the ruthenium acetylide linkers provide the right degree of coupling to the electrode to allow good conductivity on one side and to prevent quenching of the photoswitching event by the gold plasmon. Subsequently, the

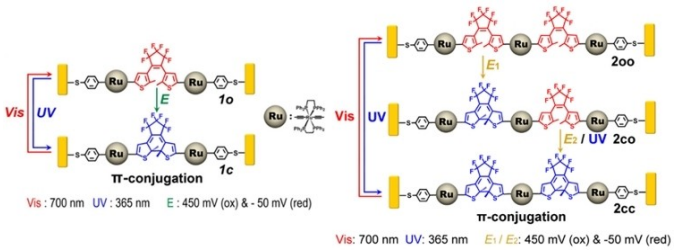

Figure 19. Orthogonally modulated isomerization of the bimetallic (left) and the trimetallic (right) complexes in the junctions. Reproduced from ref.[95b] Copyright © 2014, The Author(s).

known electrochemical cyclisation of the open state of such bimetallic-DTE adduct (*vide supra*) was achieved in the nanogap by applying a positive potential in CH_2Cl_2 solution, as attested by the resultant switching to the high conduction state. Thanks to the ruthenium fragment, this electrochemical cyclisation can be achieved at a low potential, avoiding the breakage of the Au–S bond that would occur in the case of pure organic DTE. Then, in order to explore more advanced functions, the trinuclear compound was further investigated. In addition to the one step full molecular isomerization of this trimetallic complex containing two DTE units under UV irradiation, stepwise closure could be also achieved by stepwise electrochemical and photo-stimulations or *via* a two-step electrochemical process (Figure 20).

In a further work (Figure 21), in collaboration with X. Guo, we achieved an even more challenging function by combining the rectification and the field effect transistor (FET) properties in one molecular device.[97] An unprecedented gate electric-field-induced symmetry-breaking effect with photocontrollability in an initially symmetric single-molecule junction was observed with the dinuclear Ru-DAE complex sandwiched covalently between graphene electrodes to achieve single-molecule junctions (SMJs) (Figure 21). The photoswitching property of the Ru-DAE demonstrated reproducible conductance switching under alternating visible/ultraviolet (Vis/UV) light irradiation in vacuum, consistent with the above studies. Using an ionic liquid

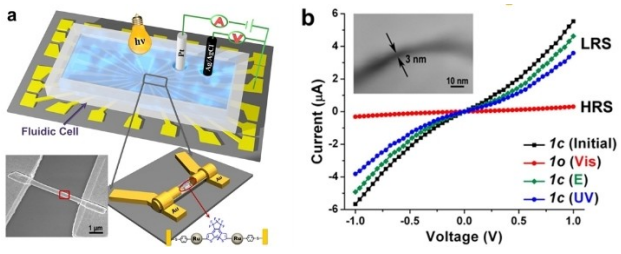

Figure 20. (a) Diagram of the functionalized nanogap devices. Inset: SEM image of a device fabricated by OWL-generated nanowire. (b) I–V characteristics of ~3 nm gap devices loaded with the closed compound, and obtained in the dark under vacuum. Black curve: initial closed compound device. Red curve: after 700 nm irradiation for 2 h to open-device. Green curve: after subsequent electrolysis of open compound at 450 mV vs Ag/AgCl for 10 min followed by −50 mV for 10 min in CH_2Cl_2 to return to closed-device. Blue curve: after 365 nm irradiation of open device for 30 min to obtain the closed-device (L/HRS: Low/High Resistance State). Inset: SEM image of a ~3 nm gap. Reproduced from ref.[96b] Copyright © 2014, The Author(s).

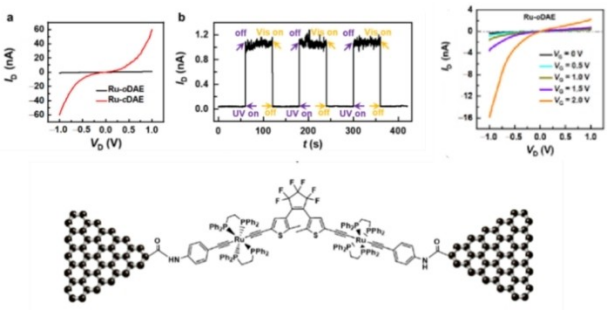

Figure 21. Reversible photoswitching and field-effect characteristics of an individual Ru-DAE SMJ. (left) Current – voltage (ID – VD) curves of individual Ru-DAEs in open-ring (dark) and closed-ring (red) forms at VG = 0 V. (middle) Real-time measurement of the current passing through a Ru-DAE molecule that switches reversibly back-and-forth between its closed-ring and open-ring forms upon exposure to ultraviolet (UV: 365 nm) and visible (Vis: 650 nm) lights, respectively. VD = 0.1 V and VG = 0 V. (right) Representative gate dependent ID-VD characteristics for the open-ring form. Adapted from ref.[97] Copyright © 2021, American Chemical Society.

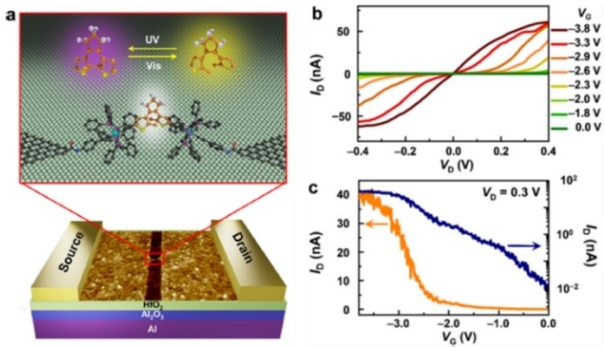

Figure 22. (a) Device diagrams of a graphene-Ru-DAE-graphene single-molecule FET. Schematic representation of the device structure. Bottom: Atomic force microscopic image of nanogapped graphene point contacts with the bottom gate. Top: Schematic of the device center that highlights the reversible isomerisation of the DAE unit between ring-open and ring-closed forms that are triggered by optical stimuli. (b) Gate-controllable charge transport in Ru-oDAE single-molecule transistors. Representative I_D–V_D curves for different values of VG. (c) Transfer characteristics for the Ru-oDAE single-molecule FET at VD = 0.3 V. Adapted from ref.[98] Copyright © 2022, The Author(s).

as gate dielectric, which has been demonstrated as an effective method to tune molecular orbital to investigate the FET behavior, it was found that the Ru-DAE SMJs exhibited obvious gate-dependent current – voltage (ID–VD) and the current passing through these junctions increases as the gate voltage (VG) becomes increasingly positive or negative, which is indicative of ambipolar characteristics. Interestingly, the open isomer output characteristics under gate electric field show clear asymmetric conductance behavior with bias dependence and the rectification directions under the positive and negative gate electric fields are opposite. More specifically, a gate controlled rectifying function (the on/off ratio reaches ~60) and a high-performance field effect (maximum on/off ratio > 100) are observed simultaneously. Both experimental and theoretical results consistently demonstrate that the initially degenerated frontier molecular orbitals localized at each Ru fragment in the open-ring Ru-DAE molecule can be tuned separately and shift asymmetrically under gate electric fields. This symmetric orbital shifting (AOS) lifts the degeneracy and breaks the molecular symmetry. In addition, this gate-controlled symmetry-breaking effect can be switched on/off by isomerizing the DAE unit between its open-ring and closed-ring forms with light stimulus. With strong conjugation and orbital delocalization between two fragments in the closed isomer state, there is no obvious AOS under different gate voltages, which implies that the symmetry is maintained throughout the molecular backbone with VG, i.e., no rectification effect appears.

Finally, still seeking alternative candidates to downsize electronics, which should be compatible with microelectronics in the future, a robust solid-state single-molecule field effect transistor architecture using graphene source/drain electrodes and a metal back-gate electrode with ultrathin high-k metal oxides as the dielectric layers was further achieved with the same Ru-DAE (Figure 22).[98] The device displayed an exceptional maximum on/off ratio exceeding three orders of magnitude. The Ru-DAE also preserves its intrinsic photoisomerisation property, which enables a reversible photoswitching function. Both experimental and theoretical results demonstrate these distinct dual-gated behaviours consistently at the single-molecule level, which helps to develop a different technology for creation of practical ultraminiaturised functional electrical circuits beyond Moore's law. Hence, all these studies demonstrated, with the help of ruthenium organometallics, new proof-of-concept and the possibility to develop multifunctional molecular devices by rational design paving the way toward real applications.

4.4. Charge Transport in Bulk Field Effect Transistors (FET)

While Pt-alkynyl semiconducting polymers have dominated the field for decades,[99] Ru alkynyl compounds were thought to be promising bulk semiconducting motifs for charge transport in FET only recently owing to their relatively low oxidation potential and their large d/π mixing orbitals not present in their Pt counterparts,. Attempts to prepare semiconducting polymers were scarcely reported[100] but the only successful outcome was provided by the Liessel's group (Scheme 10).[101] The authors tried various synthetic conditions, and they succeeded in achieving the polymers syntheses by using the methodology developed by Touchard, thanks to an aryl alkyne moiety endowed with long alkyl chains which likely favored the solubility of large intermediate oligomers. The organometallic semiconducting polymer was found to transport holes with

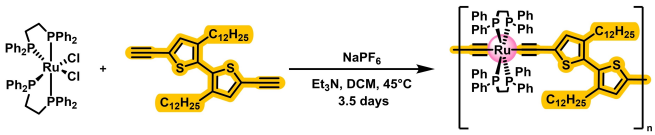

Scheme 10. Synthetic route to obtain the first example of semiconducting polymers encompassing Ru acetylide motifs.

quite poor mobility of 5×10^{-5} $cm^2V^{-1}s^{-1}$. Such low hole mobility might be explained by a lack of interchain overlap leading to limited interchain hopping, probably because of the presence of the sterically demanding *1,2-dppe* ancillary ligands. In fact, one may think that this polymer might belong to the peculiar family of the Insulated Molecular Wires (IMW).[102] Anyway, further improvement of the charge conductivity should be observed with systems featuring careful supramolecular engineering (*vide infra*).

5. Ru(II) Acetylide Compounds in Supramolecular Assemblies

Self-assembly of small molecules through multiple non-covalent interactions such as Hydrogen bonding, Halogen bonding, π-π stacking, Van der Waals interactions or metal-metal interactions is key to fabricate (multi)functional materials exhibiting *inter alia* intriguing optoelectronics features,[103] high chemical sensing abilities,[104] photochemical and electrochemical responsiveness[105] or remarkable charge transport properties.[106] In particular, supramolecular order is a prerequisite to obtaining high charge mobilities in FET.[107] Although, organic semiconducting small-molecules or covalent polymeric materials have clearly dominated the field of OPV and OFET, metal alkynyl molecules or polymers (metal = Pt, Zn) were also reported.[2b] Installation of a transition metal center within the π-conjugated system may grant the molecule/polymer with attractive features because i) the redox center could ease and facilitate the charge injection and hopping, ii) the metal could participate to the supramolecular assembly[108] through metal-metal interactions or metal-ligand interactions, and iii) the metal should allow fine tuning of the HOMO to LUMO gap through genuine d/π mixing. Consequently, Pt alkynyl derivatives were utilized as light harvesting compounds in OPV devices, while Au acetylides complexes were used for their tunable solid-state luminescence.[4a] Conversely, reports of Pt-based polyynes used as FET semiconductor are much scarcer and the moderate obtained mobilities ranged between 1.9×10^{-5} and 2.2×10^{-2} $cm^2V^{-1}s^{-1}$.[6,109]

Unlike their Pt counterparts, Ru alkynyl complexes present low oxidation potentials, promising for charge transport capabilities. In addition, in Ru alkynyl compounds, the two *1,2-diphenylphosphinoethane* (1,2-dppe) ancillary ligands provide steric shielding for the metal and stabilize the overall *trans* configurational structure. However, the steric shielding also drastically impedes intermolecular (conjugated) ligand overlap (or intimate contact) prohibiting charge hopping. Thus, the complex must be equipped with a ligand that could accommodate such a bulky coordination sphere.

We recently addressed this issue by substituting the Ru center with a Toluene Bis-Amide (TBA) motif (Figure 23).[11] As opposed to other metal acetylides supramolecular monomers, which possess amido function positioned within the long molecular axis, the two amido groups positioned outside the molecular axis confer TBA a remarkable ability to pack in a head-to-tail fashion thanks to hydrogen bond arrays running in opposite direction. We successfully anticipated that a remotely positioned TBA moiety relative to the metal center with an additional ethynyl phenyl spacer would yield strong supramolecular interactions for steric reasons since our design indeed formed supramolecular gels in low polarity solvents (Benzene, Toluene, Xylene and Mesitylene) due to H-bonds, as monitored by FTIR and VT-NMR. Also, Small Angle X-ray Scattering (SAXS) performed on a gel sample confirmed the lamellar supramolecular organization and strongly indicated the formation of a highly arranged structure where the molecules likely stood upright. The center of the lamellae contains electron rich Ru centers while the aliphatic moieties segregate from the aromatic cores and formed isolating sheaths through Van der Waals interactions and chain interdigitation (Figure 23). In other words, Ru alkynyl equipped with TBA fragments self-organized in a highly promising way for charge transport across the lamellae.

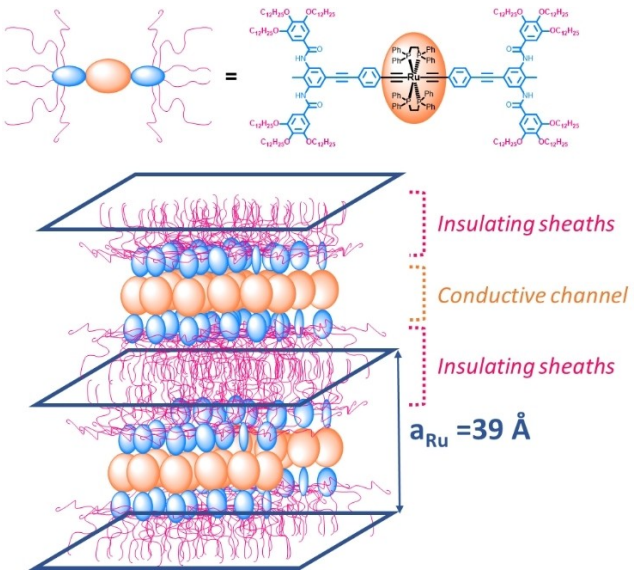

Figure 23. Supramolecular organization of the monometallic bis-acetylide prototype within the gel. The molecules arranged in lamellae with interlayer distance of 39 Å where insulating sheaths formed by aliphatic chains interdigitation isolate the electron rich supramolecular centers. Adapted with permission from ref.[11] Copyright © 2021, American Chemical Society.

More recently, our group prepared modified versions of this first Ru-based organometallic gelator in view of establishing a more reliable structure-property relationship. More precisely, we synthesized a non-symmetric monometallic compound embedding only one TBA moiety (Figure 24).[109] Although the molecule lost its gelation ability in aromatic solvent, self-assembly occurred in solution as proved by VT-NMR or FTIR, also through H-bonding interactions. Interestingly, detailed VT-NMR afforded chemical shift variations symptomatic of an *isodesmic* growth,[110] characterized by the absence of cooperativity effect. The corresponding growth enthalpy and entropy were evaluated to be $\Delta H_e = -65$ $kJ\,mol^{-1}$ and $\Delta S_e = -166$ $J\,K^{-1}\,mol^{-1}$,as classically observed in other supramolecular systems. The model also suggests that the molecules dimerized

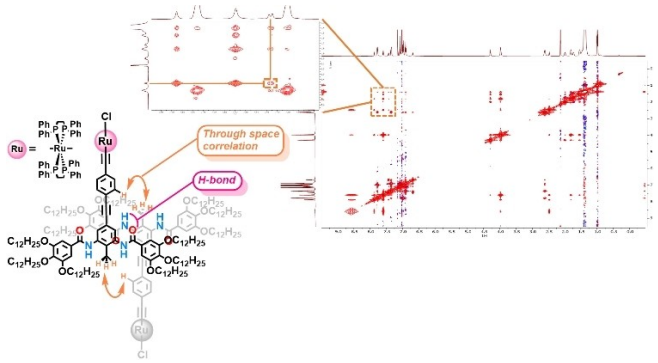

Figure 24. Schematic of the through-space correlation found in solution (C = 10 mM) indicative of a shifted head-to-tail supramolecular aggregation of the monometallic mono-alkynyl derivatives. Adapted from ref.[109] Copyright, © 2022 The Authors. European Journal of Inorganic Chemistry published by Wiley-VCH GmbH.

at room temperature, and probably in a slightly shifted head-to-tail fashion as suggested by 2D NOESY NMR experiments. Such a result well agreed with our previous assessments and led us to re-investigate the aggregation of our symmetric prototype molecule. VT-NMR experiments afforded compelling evidences that the supramolecular growth also followed an *isodesmic* process characterized by an enthalpy (entropy) of growth of $-128\ kJ\,mol^{-1}$ ($-358\ J\,K^{-1}\,mol^{-1}$). Interestingly, the growth enthalpy and entropy roughly doubled when going from the molecule embedded with one TBA unit to the compound possessing two TBA moieties, suggesting an additive relationship.

Overall, these seminal works clearly show the potential of RuII alkynyl for self-assembly and pave the way toward new organometallic supramolecular soft materials. However, there is more to be done in order to design molecules with higher self-assembly efficiencies, targeting formation of 1D, 2D or 3D supramolecular assemblies. Our current efforts are directed toward these very stimulating prospects.

6. Summary and Outlook

Ru^{II} alkynyl derivatives are original and fascinating molecules that display useful properties toward the understanding and/or the development of various domains important for applications ranging from molecular/organic electronics to photovoltaics, sensing or for the design of switchable materials.

These derivatives display light harvesting abilities due to their d/π–π* MLCT transition located in the visible range. This MLCT character can be easily tuned when the metal center is connected to a photochromic fragment, leading to light responsive organometallic dyes with high absorptivity in the visible range. The very same MLCT character turns into a strong charge transfer, which affords valuable nonlinear optical properties.

Concomitantly, the d/π mixing raises the complex HOMO energy level leading to accessible oxidation potentials useful for building innovative redox switches, for obtaining fast electron transfer interesting for memory devices and excellent charge conduction at the nanoscale and for state-of-the-art thermoelectric molecular junctions. When connected to DTE fragments, advanced multifunctional nanocircuits could be built paving the way for real applications. In bulk, hole transport measurement clearly indicated the need of a supramolecular engineering for those materials, as presented in the last part of the review.

However, despite the successful progress, there is still room for improvements and new discoveries. For example, semiconducting Donor-Acceptor (D–A) polymeric materials entailing Ru alkynyl motif as the Donor might provide molecular materials presenting not only higher charge conductivities but also absorption profiles shifted toward the Near Infrared range, a region of high interest for biological applications and optoelectronics. Novel NLO response are also expected for such D–A 1D polymers that might outperform the ones obtained with the 2D dendritic systems. This would also offer opportunities to investigate the material's dimensionality (2D vs 1D) influence onto the NLO features. Another interest in developing 1D polymers entailing Ru acetylides motifs lies in the fact that as for semiconducting polymers, such materials are easily processed through coating or printable technics. So, we are convinced that D–A polymers of Ru acetylides are appealing targets.

As they usually exhibit poor luminescence features, one might also suggest deep investigation of Ru^{II} acetylide derivatives photophysic properties, to determine the main deactivation pathway of their excited states. Such studies would certainly afford new perspectives regarding their potential use as dyes in photoacoustic, photothermal measurements or for photodynamic therapy (singlet oxygen generation). They should also provide new insights regarding the role of the metal center in multi photochromic dyes, a key step for further improvements.

As for others metal acetylides (metal = Pt^{II}, Au^{I}), Ru^{II} alkynyl compounds should be assessed for their potential (photo)cytotoxicity. Moreover, their sharp intense characteristic –C≡C– stretching vibration located at around 2050 cm^{-1} could be of great interest in Raman bioimaging, turning Ru^{II} alkynyl derivatives into Raman and redox active bio-tags. However, one should reinvent first the chemistry of Ru^{II} bis-acetylide to adapt it to biological media by proper functionalization of *1,2-dppe* ancillary ligands for instance.

Finally, supramolecular association of Ru^{II} organometallics is still in its infancy and further molecular development is required to design supramolecular material endowing multifunctionality - photochromic and/or electrochromic properties.

Altogether, we believe this contribution will help researchers to pursue the design of novel Ru^{II} alkynyl based molecular materials. There is much to do and Ru(II) acetylides hold great promises.

Acknowledgements

The authors thanks the Université de Rennes, the CNRS and Agence Nationale de la Recherche (ANR) for support.

Conflict of Interests

The authors declare no conflict of interest.

Data Availability Statement

The data that support the findings of this study are available from the corresponding author upon reasonable request.

Keywords: Ruthenium · Metal acetylide · Optical properties · Electrochemical properties · Molecular switch and devices

[1] K. A. Green, M. P. Cifuentes, M. Samoc, M. G. Humphrey, *Coord. Chem. Rev.* **2011**, *255*, 2025–2038.
[2] a) C. L. Ho, Z. Q. Yu, W. Y. Wong, *Chem. Soc. Rev.* **2016**, *45*, 5264–5295; b) L. Xu, C.-L. Ho, L. Liu, W.-Y. Wong, *Coord. Chem. Rev.* **2018**, *373*, 233–257.
[3] a) K. Costuas, S. Rigaut, *Dalton Trans.* **2011**, *40*, 5643–5658; b) S. Rigaut, *Dalton Trans.* **2013**, *42*, 15859–15863.
[4] a) C. Cuerva, M. Cano, C. Lodeiro, *Chem. Rev.* **2021**, *121*, 12966–13010; b) Y. Han, Z. Gao, C. Wang, R. Zhong, F. Wang, *Coord. Chem. Rev.* **2020**, *414*, 213300.
[5] A. Haque, R. A. Al-Balushi, M. S. Khan, *J. Organomet. Chem.* **2019**, *897*, 95–106.
[6] L. Yan, Y. Zhao, X. Wang, X. Z. Wang, W. Y. Wong, Y. Liu, W. Wu, Q. Xiao, G. Wang, X. Zhou, W. Zeng, C. Li, X. Wang, H. Wu, *Macromol. Rapid Commun.* **2012**, *33*, 603–609.
[7] a) N. J. Long in *Molecular Design and Applications of Photofunctional Polymers and Materials, chapter 4* (Eds.: W. Y. Wong, A. S. Abd-El-Aziz), RSC Publishing, **2012**, 85–129; b) P. J. Low, *Coord. Chem. Rev.* **2013**, *257*, 1507–1532; c) M. C. Leech, I. R. Crossley, *Dalton Trans.* **2018**, *47*, 4428–4432.
[8] a) P. Haquette, N. Pirio, D. Touchard, L. Toupet, P. H. Dixneuf, *Chem. Commun.* **1993**, 163–165; b) Z. Atherton, C. W. Faulkner, S. L. Ingham, A. K. Kakkar, M. S. Khan, J. Lewis, Nicholas J. Long, P. R. Raithby, *J. Organomet. Chem.* **1993**, *462*, 265–270.
[9] L. A. Miller-Clark, T. Ren, *J. Organomet. Chem.* **2021**, *951*, 122003.
[10] M. A. Fox, J. E. Harris, S. Heider, V. Pérez-Gregorio, M. E. Zakrzewska, J. D. Farmer, D. S. Yufit, J. A. K. Howard, P. J. Low, *J. Organomet. Chem.* **2009**, *694*, 2350–2358.
[11] O. Galangau, D. Daou, N. El Beyrouti, E. Caytan, C. Meriadec, F. Artzner, S. Rigaut, *Inorg. Chem.* **2021**, *60*, 11474–11484.
[12] A. Colombo, C. Dragonetti, D. Roberto, R. Ugo, L. Falciola, S. Luzzati, D. Kotowski, *Organometallics* **2011**, *30*, 1279–1282.
[13] S. De Sousa, L. Ducasse, B. Kauffmann, T. Toupance, C. Olivier, *Chem. Eur. J.* **2014**, *20*, 7017–7024.
[14] F. Nisic, A. Colombo, C. Dragonetti, E. Garoni, D. Marinotto, S. Righetto, F. De Angelis, M. G. Lobello, P. Salvatori, P. Biagini, F. Melchiorre, *Organometallics* **2014**, *34*, 94–104.
[15] S. De Sousa, S. Lyu, L. Ducasse, T. Toupance, C. Olivier, *J. Mater. Chem. A* **2015**, *3*, 18256–18264.
[16] S. Lyu, Y. Farré, L. Ducasse, Y. Pellegrin, T. Toupance, C. Olivier, F. Odobel, *RSC Adv.* **2016**, *6*, 19928–19936.
[17] J. Massin, S. Lyu, M. Pavone, A. B. Munoz-Garcia, B. Kauffmann, T. Toupance, M. Chavarot-Kerlidou, V. Artero, C. Olivier, *Dalton Trans.* **2016**, *45*, 12539–12547.
[18] S. Zhang, Y. Sheng, G. Wei, Y. Quan, Y. Cheng, C. Zhu, *J. Polym. Sci.* **2014**, *52*, 1686–1692.
[19] J.-L. Fillaut, J. Perruchon, *Inorg. Chem. Commun.* **2002**, *5*, 1048–1051.
[20] J.-L. Fillaut, J. Andries, L. Toupet, J. P. Desvergne, *Chem. Commun.* **2005**, *23*, 2924–2926.
[21] K. Aratsu, R. Takeya, B. R. Pauw, M. J. Hollamby, Y. Kitamoto, N. Shimizu, H. Takagi, R. Haruki, S. I. Adachi, S. Yagai, *Nat. Commun.* **2020**, *11*, 1623.
[22] J.-L. Fillaut, J. Andriès, R. D. Marwaha, P.-H. Lanoë, O. Lohio, L. Toupet, J. A. Gareth Williams, *J. Organomet. Chem.* **2008**, *693*, 228–234.
[23] E. Garmire, *Opt. Express* **2013**, *21*, 30532–30544.
[24] B. Weigelin, G. J. Bakker, P. Friedl, *J. Cell. Sci.* **2016**, *129*, 245–255.
[25] a) G. S. He, L.-S. Tan, Q. Zheng, P. N. Prasad, *Chem. Rev.* **2008**, *108*, 1245–1330; b) T.-C. Lin, S.-J. Chung, K.-S. Kim, X. Wang, G. S. He, J. Swiatkiewicz, H. E. Pudavar, P. N. Prasad, *Polymers for Photonics Applications II*, vol. 161 (Ed.: K.-S. Lee), Springer Berlin, Heidelberg **2003**, 157–193.
[26] a) J. Liu, C. Ouyang, F. Huo, W. He, A. Cao, *Dyes Pigm.* **2020**, *181*, 108509; b) S. R. Marder, *Chem. Commun.* **2006**, 131–134; c) M. Li, Y. Li, H. Zhang, S. Wang, Y. Ao, Z. Cui, *J. Mater. Chem. C* **2017**, *5*, 4111–4122.
[27] For key articles see: a) A. M. McDonagh, M. G. Humphrey, M. Samoc, B. Luther-Davies, S. Houbrechts, T. Wada, H. Sasabe, A. Persoons, *J. Am. Chem. Soc.* **1999**, *121*, 1405–1406; b) S. K. Hurst, M. P. Cifuentes, J. P. L. Morrall, N. T. Lucas, I. R. Whittall, M. G. Humphrey, I. Asselberghs, A. Persoons, M. Samoc, B. Luther-Davies, A. C. Willis, *Organometallics* **2001**, *20*, 4664–4675; c) S. K. Hurst, M. G. Humphrey, T. Isoshima, K. Wostyn, I. Asselberghs, K. Clays, A. Persoons, M. Samoc, B. Luther-Davies, *Organometallics* **2002**, *21*, 2024–2026; d) M. P. Cifuentes, C. E. Powell, J. P. Morrall, A. M. McDonagh, N. T. Lucas, M. G. Humphrey, M. Samoc, S. Houbrechts, I. Asselberghs, K. Clays, A. Persoons, T. Isoshima, *J. Am. Chem. Soc.* **2006**, *128*, 10819–10832; e) T. Gulliver, M. Samoc, N. Gauthier, M. P. Cifuentes, F. Paul, C. Lapinte, M. G. Humphrey, *Angew. Chem. Int. Ed.* **2006**, *45*, 7376–7379; For authoritative reviews see (and references therein): f) L. Zhang, M. G. Humphrey, *Coord. Chem. Rev.* **2022**, *473*, 214820; g) M. G. Humphrey, *Aust. J. Chem.* **2018**, *71*, 731–742; h) C. E. Powell, M. G. Humphrey, *Coord. Chem. Rev.* **2004**, *248*, 725–756; i) M. P. Cifuentes, M. G. Humphrey, *J. Organomet. Chem.* **2004**, *689*, 3968–3981; j) J. P. Morrall, G. T. Dalton, M. G. Humphrey, M. Samoc, *Adv. Organomet. Chem.* **2007**, *55*, 61–136; k) M. G. Humphrey, T. Schwich, P. J. West, M. P. Cifuentes, M. Samoc, *Comprehensive Inorganic Chemistry II*, vol. 8 (Eds.: J. Reedijk, K. R. Poeppelmeier), Elsevier B. V., Amsterdam, **2013**, 781–835.
[28] A. Colombo, F. Nisic, C. Dragonetti, D. Marinotto, I. P. Oliveri, S. Righetto, M. G. Lobello, F. De Angelis, *Chem. Commun.* **2014**, *50*, 7986–7989.
[29] R. J. Durand, S. Gauthier, S. Achelle, T. Groizard, S. Kahlal, J. Y. Saillard, A. Barsella, N. Le Poul, F. R. Le Guen, *Dalton Trans.* **2018**, *47*, 3965–3975.
[30] M. Morshedi, M. S. Kodikara, T. C. Corkery, S. K. Hurst, S. S. Chavan, E. Kulasekera, R. Stranger, M. Samoc, S. Van Cleuvenbergen, I. Asselberghs, K. Clays, M. P. Cifuentes, M. G. Humphrey, *Chem. Eur. J.* **2018**, *24*, 16332–16341.
[31] a) A. Colombo, C. Dragonetti, D. Marinotto, S. Righetto, G. Griffini, S. Turri, H. Akdas-Kilig, J.-L. Fillaut, A. Amar, A. Boucekkine, C. Katan, *Dalton Trans.* **2016**, *45*, 11052–11060; b) J.-L. Fillaut, *Display and Imaging* **2016**, *2*, 115–134.
[32] P. A. Shaw, E. Forsyth, F. Haseeb, S. Yang, M. Bradley, M. Klausen, *Front. Chem.* **2022**, *10*, 921354.
[33] X. Zhang, L. Shi, M. A. Fox, A. Barlow, M. Morshedi, M. P. Cifuentes, M. G. Humphrey, O. Mongin, F. Paul, C. O. Paul-Roth, *Dyes Pigm.* **2021**, *188*, 109155.
[34] L. Zhang, M. Morshedi, M. G. Humphrey, *Angew. Chem. Int. Ed.* **2022**, *61*, e202116181.
[35] J. Perez-Moreno, M. G. Kuzyk, *Adv. Mater.* **2011**, *23*, 1428–1432.
[36] L. Zhang, M. Morshedi, M. S. Kodikara, M. G. Humphrey, *Angew. Chem. Int. Ed.* **2022**, *61*, e202208168.
[37] E. Di Piazza, A. Merhi, L. Norel, S. Choua, P. Turek, S. Rigaut, *Inorg. Chem.* **2015**, *54*, 6347–6355.
[38] a) L. Norel, K. Bernot, M. Feng, T. Roisnel, A. Caneschi, R. Sessoli, S. Rigaut, *Chem. Commun.* **2012**, *48*, 3948–3950; b) L. Norel, M. Feng, K. Bernot, T. Roisnel, T. Guizouarn, K. Costuas, S. Rigaut, *Inorg. Chem.* **2014**, *53*, 2361–2363.
[39] a) M. Irie, T. Fulcaminato, K. Matsuda, S. Kobatake, *Chem. Rev.* **2014**, *114*, 12174–12277; b) M. Berberich, A. M. Krause, M. Orlandi, F. Scandola, F. Wurthner, *Angew. Chem. Int. Ed.* **2008**, *47*, 6616–6619.
[40] a) M. Natali, S. Giordani, *Chem. Soc. Rev.* **2012**, *41*, 4010–4029; b) Q. Zou, X. Li, J. J. Zhang, J. Zhou, B. B. Sun, H. Tian, *Chem. Commun.* **2012**, *48*, 2095–2097.
[41] J. Boixel, V. Guerchais, H. Le Bozec, D. Jacquemin, A. Amar, A. Boucekkine, A. Colombo, C. Dragonetti, D. Marinotto, D. Roberto, S. Righetto, R. De Angelis, *J. Am. Chem. Soc.* **2014**, *136*, 5367–5375.

[42] D. Pinkowicz, M. Ren, L. M. Zheng, S. Sato, M. Hasegawa, M. Morimoto, M. Irie, B. K. Breedlove, G. Cosquer, K. Katoh, M. Yamashita, *Chem. Eur. J.* **2014**, *20*, 12502–12513.

[43] a) M. M. Russew, S. Hecht, *Adv. Mater.* **2010**, *22*, 3348–3360; b) E. Orgiu, P. Samori, *Adv. Mater.* **2014**, *26*, 1827–1845; c) F. B. Meng, Y. M. Hervault, Q. Shao, B. H. Hu, L. Norel, S. Rigaut, X. D. Chen, *Nat. Commun.* **2014**, *5*, 9; d) F. B. Meng, Y. M. Hervault, L. Norel, K. Costuas, C. Van Dyck, V. Geskin, J. Cornil, H. H. Hng, S. Rigaut, X. D. Chen, *Chem. Sci.* **2012**, *3*, 3113–3118.

[44] a) W. R. Browne, J. J. D. de Jong, T. Kudernac, M. Walko, L. N. Lucas, K. Uchida, J. H. van Esch, B. L. Feringa, *Chem. Eur. J.* **2005**, *11*, 6414–6429; b) G. Guirado, C. Coudret, M. Hliwa, J. P. Launay, *J. Phys. Chem. B* **2005**, *109*, 17445–17459; c) Y. F. Liu, C. M. Ndiaye, C. Lagrost, K. Costuas, S. Choua, P. Turek, L. Norel, S. Rigaut, *Inorg. Chem.* **2014**, *53*, 8172–8188.

[45] C. T. Poon, W. H. Lam, V. W. W. Yam, *Chem. Eur. J.* **2013**, *19*, 3467–3476.

[46] T. Okuyama, Y. Tani, K. Miyake, Y. Yokoyama, *J. Org. Chem.* **2007**, *72*, 1634–1638.

[47] a) F. M. Raymo, *Phys. Chem. Chem. Phys.* **2013**, *15*, 14840–14850; b) C. Li, H. Yan, L. X. Zhao, G. F. Zhang, Z. Hu, Z. L. Huang, M. Q. Zhu, *Nat. Commun.* **2014**, *5*, 5709.

[48] V. Blanco, D. A. Leigh, V. Marcos, *Chem. Soc. Rev.* **2015**, *44*, 5341–5370.

[49] a) B. Li, J.-Y. Wang, H.-M. Wen, L.-X. Shi, Z.-N. Chen, *J. Am. Chem. Soc.* **2012**, *134*, 16059–16067; b) G.-T. Xu, B. Li, J.-Y. Wang, D.-B. Zhang, Z.-N. Chen, *Chem. Eur. J.* **2015**, *21*, 3318–3326; c) J. X. Chen, J. Y. Wang, Q. C. Zhang, Z. N. Chen, *Inorg. Chem.* **2017**, *56*, 13257–13266; d) H. L. Wong, C. H. Tao, N. Zhu, V. W. Yam, *Inorg. Chem.* **2011**, *50*, 471–481.

[50] Y. M. Hervault, C. M. Ndiaye, L. Norel, C. Lagrost, S. Rigaut, *Org. Lett.* **2012**, *14*, 4454–4457.

[51] a) Y. F. Liu, C. Lagrost, K. Costuas, N. Tchouar, H. Le Bozec, S. Rigaut, *Chem. Commun.* **2008**, 6117–6119; b) Y. M. Hervault, C. M. Ndiaye, L. Norel, C. Lagrost, S. Rigaut, *Org. Lett.* **2012**, *14*, 4454–4457; c) T. Nakashima, Y. Kajiki, S. Fukumoto, M. Taguchi, S. Nagao, S. Hirota, T. Kawai, *J. Am. Chem. Soc.* **2012**, *134*, 19877–19883; d) M. Akita, *Organometallics* **2011**, *30*, 43–51.

[52] E. C. Harvey, B. L. Feringa, J. G. Vos, W. R. Browne, M. T. Pryce, *Coord. Chem. Rev.* **2015**, *282*, 77–86.

[53] Y. Tanaka, T. Ishisaka, A. Inagaki, T. Koike, C. Lapinte, M. Akita, *Chem. Eur. J.* **2010**, *16*, 4762–4776.

[54] K. Green, M. Cifuentes, T. Corkery, M. Samoc, M. G. Humphrey, *Angew. Chem. Int. Ed.* **2009**, *48*, 7867–7870.

[55] a) M. C. Walkey, L. T. Byrne, M. J. Piggott, P. J. Low, G. A. Koutsantonis, *Dalton Trans.* **2015**, *44*, 8812–8815; b) D. Jago, A. R. Langley, S. G. Eaves, M. C. Walkey, T. Pulbrook, S. A. Moggach, M. J. Piggott, P. J. Low, G. A. Koutsantonis, *Dalton Trans.* **2022**, *52*, 185–200.

[56] C. Shen, X. He, L. Toupet, L. Norel, S. Rigaut, J. Crassous, *Organometallics* **2018**, *37*, 697–705.

[57] a) L. Motiei, D. Margulies, *Acc. Chem. Res.* **2023**, *56*, 1803–1814; b) J. A. Kitchen, R. Parkesh, E. B. Veale, T. Gunnlaugsson, *Supramolecular Chemistry: From Molecules to Nanomaterials*, vol. 5, Eds.: P. A. Gale, J. W. Steed), Wiley-Blackwell, Oxford, **2012**, 1–27; c) Y. Hasegawa, T. Nakagawa, T. Kawai, *Coord. Chem. Rev.* **2010**, *254*, 2643–2651; d) P. Audebert, F. Miomandre, *Chem. Sci.* **2013**, *4*, 575–584.

[58] a) A. Zampetti, A. Minotto, F. Cacialli, *Adv. Funct. Mater.* **2019**, *29*, 1807623; b) D. Zou, J. Zhang, Y. Cui, G. Qian, *Dalton Trans.* **2019**, *48*, 6669–6675; c) Y. Ning, M. Zhu, J.-L. Zhang, *Coord. Chem. Rev.* **2019**, *399*, 213028; d) J. Xu, A. Gulzar, P. Yang, H. Bi, D. Yang, S. Gai, F. He, J. Lin, B. Xing, D. Jin, *Coord. Chem. Rev.* **2019**, *381*, 104–134.

[59] A. M. Smith, M. C. Mancini, S. Nie, *Nat.ure Nanotech.* **2009**, *4*, 710–711.

[60] A. T. Bui, M. Beyler, A. Grichine, A. Duperray, J.-C. Mulatier, Y. Guyot, C. Andraud, R. Tripier, S. Brasselet, O. Maury, *Chem. Commun.* **2017**, *53*, 6005–6008.

[61] L. Norel, O. Galangau, H. Al Sabea, S. Rigaut, *ChemPhotoChem* **2021**, *5*, 393–405.

[62] a) A. D'Aleo, F. Pointillart, L. Ouahab, C. Andraud, O. Maury, *Coord. Chem. Rev.* **2012**, *256*, 1604–1620; b) E. G. Moore, A. P. S. Samuel, K. N. Raymond, *Acc. Chem. Res.* **2009**, *42*, 542–552; c) J.-C. G. Bünzli, *Coord. Chem. Rev.* **2015**, *293–294*, 19–47.

[63] E. Di Piazza, L. Norel, K. Costuas, A. Bourdolle, O. Maury, S. Rigaut, *J. Am. Chem. Soc.* **2011**, *133*, 6174–6176.

[64] L. Norel, E. Di Piazza, M. Feng, A. Vacher, X. Y. He, T. Roisnel, O. Maury, S. Rigaut, *Organometallics* **2014**, *33*, 4824–4835.

[65] H. Al Sabea, L. Norel, O. Galangau, H. Hijazi, R. Métivier, T. Roisnel, O. Maury, C. Bucher, F. Riobé, S. Rigaut, *J. Am. Chem. Soc.* **2019**, *141*, 20026–20030.

[66] P. Selvanathan, E. Tufenkjian, O. Galangau, T. Roisnel, F. Riobe, O. Maury, L. Norel, S. Rigaut, *Inorg. Chem.* **2023**, *62*, 2049–2057.

[67] L. Norel, C. Tourbillon, J. Warnan, J. F. Audibert, Y. Pellegrin, F. Miomandre, F. Odobel, S. Rigaut, *Dalton Trans.* **2018**, *47*, 8364–8374.

[68] X. Zhang, S. Abid, L. Shi, J. A. G. Williams, M. A. Fox, F. Miomandre, C. Tourbillon, J. F. Audibert, O. Mongin, F. Paul, C. O. Paul-Roth, *Dalton Trans.* **2019**, *48*, 11897–11911.

[69] M. Murai, M. Sugimoto, M. Akita, *Dalton Trans.* **2013**, *42*, 16108–16120.

[70] a) J. C. Love, L. A. Estroff, J. K. Kriebel, R. G. Nuzzo, G. M. Whitesides, *Chem. Rev.* **2005**, *105*, 1103–1170; b) C. Vericat, M. E. Vela, G. Benitez, P. Carro, R. C. Salvarezza, *Chem. Soc. Rev.* **2010**, *39*, 1805–1834; c) M. D. Porter, T. B. Bright, D. L. Allara, C. E. D. Chidsey, *J. Am. Chem. Soc.* **1987**, *109*, 3559–3568; d) A. L. Eckermann, D. J. Feld, J. A. Shaw, T. J. Meade, *Coord. Chem. Rev.* **2010**, *254*, 1769–1802.

[71] a) H. Qi, S. Sharma, Z. Li, G. L. Snider, A. O. Orlov, C. S. Lent, T. P. Fehlner, *J. Am. Chem. Soc.* **2003**, *125*, 15250–15259.

[72] a) G. Grelaud, N. Gauthier, Y. Luo, F. Paul, B. Fabre, F. Barriere, S. Ababou-Girard, T. Roisnel, M. G. Humphrey, *J. Phys. Chem. C* **2014**, *118*, 3680–3695; b) N. Gauthier, G. Argouarch, F. Paul, M. G. Humphrey, L. Toupet, S. Ababou-Girard, H. Sabbah, P. Hapiot, B. Fabre, *Adv. Mater.* **2008**, *20*, 1952–1956.

[73] A. Mulas, Y.-M. Hervault, X. He, E. Di Piazza, L. Norel, S. Rigaut, C. Lagrost, *Langmuir* **2015**, *31*, 7138–7147.

[74] a) T. C. Lee, D. J. Hounihan, R. Colorado, J. S. Park, T. R. Lee, *J. Phys. Chem. B* **2004**, *108*, 2648–2653; b) J. J. Stapleton, T. A. Daniel, S. Uppili, O. M. Cabarcos, J. Naciri, R. Shashidhar, D. L. Allara, *Langmuir* **2005**, *21*, 11061–11070.

[75] a) C. Amatore, E. Maisonhaute, B. Schollhorn, J. Wadhawan, *Chemphyschem* **2007**, *8*, 1321–1329; b) C. P. Chen, W. R. Luo, C. N. Chen, S. M. Wu, S. Hsieh, C. M. Chiang, T. Y. Dong, *Langmuir* **2013**, *29*, 3106–3115; c) H. O. Finklea, D. D. Hanshew, *J. Am. Chem. Soc.* **1992**, *114*, 3173–3181; d) J. F. Smalley, H. O. Finklea, C. E. D. Chidsey, M. R. Linford, S. E. Creager, J. P. Ferraris, K. Chalfant, T. Zawodzinsk, S. W. Feldberg, M. D. Newton, *J. Am. Chem. Soc.* **2003**, *125*, 2004–2013; e) K. Weber, L. Hockett, S. Creager, *J. Phys. Chem. B* **1997**, *101*, 8286–8291.

[76] S. E. Creager, G. K. Rowe, *J. Electroanal. Chem.* **1997**, *420*, 291–299.

[77] J. S. Lindsey, D. F. Bocian, *Acc. Chem. Res.* **2011**, *44*, 638–650.

[78] H. Zhu, S. J. Pookpanratana, J. Y. Bonevich, S. N. Natoli, C. A. Hacker, T. Ren, J. S. Suehle, C. A. Richter, Q. L. Li, *ACS Appl. Mater. Interfaces* **2015**, *7*, 27306–27313.

[79] a) A. Mulas, Y.-M. Hervault, L. Norel, S. Rigaut, C. Lagrost, *ChemElectroChem* **2015**, *2*, 1799–1805; b) X. He, C. Lagrost, L. Norel, S. Rigaut, *Polyhedron* **2018**, *140*, 169–180.

[80] a) T. C. Pijper, T. Kudernac, N. Katsonis, M. van der Maas, B. L. Feringa, B. J. van Wees, *Nanoscale* **2013**, *5*, 9277–9282; b) T. C. Pijper, T. Kudernac, W. R. Browne, B. L. Feringa, *J. Phys. Chem. C* **2013**, *117*, 17623–17632; c) V. D. Cabanes, C. Van Dyck, S. Osella, D. Cornil, J. Cornil, *ACS. Appl. Mater. Interfaces* **2021**, *13*, 27737–27748.

[81] A. Mulas, X. He, Y. M. Hervault, L. Norel, S. Rigaut, C. Lagrost, *Chem. Eur. J.* **2017**, *23*, 10205–10214.

[82] a) D. Xiang, X. L. Wang, C. C. Jia, T. Lee, X. F. Guo, *Chem. Rev.* **2016**, *116*, 4318–4440; b) S. V. Aradhya, L. Venkataraman, *Nat. Nanotech.* **2013**, *8*, 399–410; c) H. Song, Y. Kim, Y. H. Jang, H. Jeong, M. A. Reed, T. Lee, *Nature* **2009**, *462*, 1039–1043; d) S. H. Choi, B. Kim, C. D. Frisbie, *Science* **2008**, *320*, 1482–1486; e) X. D. Cui, A. Primak, X. Zarate, J. Tomfohr, O. F. Sankey, A. L. Moore, T. A. Moore, D. Gust, G. Harris, S. M. Lindsay, *Science* **2001**, *294*, 571–574; f) J. Chen, M. A. Reed, A. M. Rawlett, J. M. Tour, *Science* **1999**, *286*, 1550–1552; g) Z. J. Donhauser, B. A. Mantooth, K. F. Kelly, L. A. Bumm, J. D. Monnell, J. J. Stapleton, D. W. Price, A. M. Rawlett, D. L. Allara, J. M. Tour, P. S. Weiss, *Science* **2001**, *292*, 2303–2307; h) C. Joachim, J. K. Gimzewski, A. Aviram, *Nature* **2000**, *408*, 541–548; i) M. Ratner, *Nat. Nanotech.* **2013**, *8*, 378–381.

[83] a) J. M. Tour, *Acc. Chem. Res.* **2000**, *33*, 791–804; b) D. K. James, J. M. Tour, *Chem. Mater.* **2004**, *16*, 4423–4435.

[84] M. Mayor, C. Hänisch, H. B. Weber, J. Reichert, D. Beckmann, *Angew. Chem. Int. Ed.* **2002**, *41*, 1183–1186.

[85] a) H. Zhu, S. J. Pookpanratana, J. E. Bonevich, S. N. Natoli, C. A. Hacker, T. Ren, J. S. Suehle, C. A. Richter, Q. Li, *ACS Appl. Mater. Interfaces* **2015**, *7*, 27306–27313; b) F. Schwarz, G. Kastlunger, F. Lissel, C. Egler-Lucas, S. N. Semenov, K. Venkatesan, H. Berke, R. Stadler, E. Lortscher, *Nat. Nanotech.* **2016**, *11*, 170–176; c) L. Luo, A. Benameur, P. Brignou, S. H. Choi, S. Rigaut, C. D. Frisbie, *J. Phys. Chem. C* **2011**, *115*, 19955–19961; d) B. Kim, J. M. Beebe, C. Olivier, S. Rigaut, D. Touchard, J. G. Kushmerick, X.-Y. Zhu, C. Daniel Frisbie, *J. Phys. Chem. C* **2007**, *111*, 7521–7526; e) O. A. Al-Owaedi, D. C. Milan, M.-C. Oerthel, S. Bock, D. S.

Yufit, J. A. K. Howard, S. J. Higgins, R. J. Nichols, C. J. Lambert, M. R. Bryce, P. J. Low, *Organometallics* **2016**, *35*, 2944–2954; f) S. Bock, O. A. Al-Owaedi, S. G. Eaves, D. C. Milan, M. Lemmer, B. W. Skelton, H. M. Osorio, R. J. Nichols, S. J. Higgins, P. Cea, N. J. Long, T. Albrecht, S. Martin, C. J. Lambert, P. J. Low, *Chem. Eur. J.* **2017**, *23*, 2133–2143; g) S. Marques-Gonzalez, D. S. Yufit, J. A. Howard, S. Martin, H. M. Osorio, V. M. Garcia-Suarez, R. J. Nichols, S. J. Higgins, P. Cea, P. J. Low, *Dalton Trans.* **2013**, *42*, 338–341; h) J. Y. Ajit, K. Mahapatro, T. Ren, D. B. Janes, *Nano Lett.* **2008**, 2131–2136; i) H.-M. Wen, Y. Yang, X.-S. Zhou, J.-Y. Liu, D.-B. Zhang, Z.-B. Chen, J.-Y. Wang, Z.-N. Chen, Z.-Q. Tian, *Chem. Sci.* **2013**, *4*, 2471; j) M. Akita, Y. Tanaka, *Coord. Chem. Rev.* **2022**, *461*, 214501; k) D. C. Milan, A. Vezzoli, I. J. Planje, P. J. Low, *Dalton Trans.* **2018**, *47*, 14125–14138; l) Y. Tanaka, *Dalton Trans.* **2024**, *53*, 8512–8523.

[86] K. Sugimoto, Y. Tanaka, S. Fujii, T. Tada, M. Kiguchi, M. Akita, *Chem. Commun.* **2016**, *52*, 5796–5799.

[87] Y. Tanaka, Y. Kato, T. Tada, S. Fujii, M. Kiguchi, M. Akita, *J. Am. Chem. Soc.* **2018**, *140*, 10080–10084.

[88] L.-Y. Zhang, P. Duan, J.-Y. Wang, Q.-C. Zhang, Z.-N. Chen, *J. Phys. Chem. C* **2019**, *123*, 5282–5288.

[89] a) A. Yashiro, Y. Tanaka, T. Tada, S. Fujii, T. Nishino, M. Akita, *Chem. Eur. J.* **2021**, *27*, 9666–9673; b) Y. Tanaka, Y. Kato, K. Sugimoto, R. Kawano, T. Tada, S. Fujii, M. Kiguchi, M. Akita, *Chem. Sci.* **2021**, *12*, 4338–4344.

[90] R. Ezquerra, S. G. Eaves, S. Bock, B. W. Skelton, F. Pérez-Murano, P. Cea, S. Martín, P. J. Low, *J. Mater. Chem. C* **2019**, *7*, 6630–6640.

[91] a) M. Naher, D. C. Milan, O. A. Al-Owaedi, I. J. Planje, S. Bock, J. Hurtado-Gallego, P. Bastante, Z. M. Abd Dawood, L. Rincon-Garcia, G. Rubio-Bollinger, S. J. Higgins, N. Agrait, C. J. Lambert, R. J. Nichols, P. J. Low, *J. Am. Chem. Soc.* **2021**, *143*, 3817–3829; b) S. Park, J. Jang, Y. Tanaka, H. J. Yoon, *Nano Lett.* **2022**, *22*, 9693–9699.

[92] Y. Tanaka, *Chem. Eur. J.* **2023**, *29*, e202300472.

[93] a) G. Vives, J. M. Tour, *Tet. Lett.* **2009**, *50*, 1427–1430; b) G. Vives, J. M. Tour, *Acc. Chem. Res.* **2009**, *42*, 473–487.

[94] D. Xiang, X. Wang, C. Jia, T. Lee, X. Guo, *Chem. Rev.* **2016**, *116*, 4318–4440.

[95] O. Galangau, L. Norel, S. Rigaut, *Dalton Trans* **2021**, ***50***, 17879–17891.

[96] a) F. Meng, Y.-M. Hervault, L. Norel, K. Costuas, C. Van Dyck, V. Geskin, J. Cornil, H. H. Hng, S. Rigaut, X. Chen, *Chem. Sci.* **2012**, *3*, 3113; b) F. Meng, Y. M. Hervault, Q. Shao, B. Hu, L. Norel, S. Rigaut, X. Chen, *Nat. Commun.* **2014**, *5*, 3023.

[97] N. Xin, C. Hu, H. Al Sabea, M. Zhang, C. Zhou, L. Meng, C. Jia, Y. Gong, Y. Li, G. Ke, X. He, P. Selvanathan, L. Norel, M. A. Ratner, Z. Liu, S. Xiao, S. Rigaut, H. Guo, X. Guo, *J. Am. Chem. Soc.* **2021**, *143*, 20811–20817.

[98] L. Meng, N. Xin, C. Hu, H. A. Sabea, M. Zhang, H. Jiang, Y. Ji, C. Jia, Z. Yan, Q. Zhang, L. Gu, X. He, P. Selvanathan, L. Norel, S. Rigaut, H. Guo, S. Meng, X. Guo, *Nat. Commun.* **2022**, *13*, 1410.

[99] C. L. Ho, Z. Q. Yu, W. Y. Wong, *Chem. Soc. Rev.* **2016**, *45*, 5264–5295.

[100] a) Y. Zhu, D. B. Millet, M. O. Wolf, S. J. Rettig, *Organometallics* **1999**, *18* 1930–1938; b) C. W. Faulkner, M. S. Khan, J. Lewis, N. J. Long, P. R. Raithby, *J. Organomet. Chem.* **1994**, *482*, 139–145.

[101] P.-Y. Ho, H. Komber, K. Horatz, T. Tsuda, S. C. B. Mannsfeld, E. Dmitrieva, O. Blacque, U. Kraft, H. Sirringhaus, F. Lissel, *Polym. Chem.* **2020**, *11*, 472–479.

[102] a) H. Masai, J. Terao, Y. Tsuji *Tet. Lett.* **2014**, *55*, 4035–4043; b) D. B. Amabilino, D. K. Smith, J. W. Steed, *Chem. Soc. Rev.* **2017**, *46*, 2404–2420.

[103] S. S. Babu, S. Prasanthkumar, A. Ajayaghosh, *Angew. Chem. Int. Ed.* **2012**, *51*, 1766–1776.

[104] a) A. Y. Tam, V. W. Yam, *Chem. Soc. Rev.* **2013**, *42*, 1540–1567; b) S. Panja, D. J. Adams, *Chem. Soc. Rev.* **2021**, *50*, 5165–5200; c) C. D. Jones, J. W. Steed, *Chem. Soc. Rev.* **2016**, *45*, 6546–6596.

[105] M. Hasegawa, M. Iyoda, *Chem. Soc. Rev.* **2010**, *39*, 2420–2427.

[106] a) Y. Yuan, G. Giri, A. L. Ayzner, A. P. Zoombelt, S. C. Mannsfeld, J. Chen, D. Nordlund, M. F. Toney, J. Huang, Z. Bao, *Nat. Commun.* **2014**, *5*, 3005; b) Z. B. Henson, K. Mullen, G. C. Bazan, *Nat. Chem.* **2012**, *4*, 699–704; c) H. Minemawari, T. Yamada, H. Matsui, J. Tsutsumi, S. Haas, R. Chiba, R. Kumai, T. Hasegawa, *Nature* **2011**, *475*, 364–367.

[107] D. Zhong, Y. Ying, M. Gui, C. Wang, H. Zhong, H. Zhao, F. Wang, *J. Organomet. Chem.* **2021**, *933*, 121632.

[108] a) L. Yan, C. Li, L. Cai, K. Shi, W. Tang, W. Qu, C.-L. Ho, G. Yu, J. Li, X. Wang, *J. Organomet. Chem.* **2017**, *846*, 269–276; b) S. J. Bradberry, G. Dee, O. Kotova, C. P. McCoy, T. Gunnlaugsson, *Chem. Commun.* **2019**, *55*, 1754–1757; c) Q. Wang, Z. He, A. Wild, H. Wu, Y. Cao, S. S. U, C. H. Chui, W. Y. Wong, *Chem. Asian J.* **2011**, *6*, 1766–1777.

[109] O. Galangau, E. Caytan, W. T. Gallonde, I. de Waele, F. Camerel, S. Rigaut, *Eur. J. Inorg. Chem.* **2022**, *26*, e202200579.

[110] M. M. Smulders, M. M. Nieuwenhuizen, T. F. de Greef, P. van der Schoot, A. P. Schenning, E. W. Meijer, *Chem. Eur. J.* **2010**, *16*, 362–367.

Manuscript received: July 24, 2024
Accepted manuscript online: September 27, 2024
Version of record online: ■■, ■■

REVIEW

In this contribution, we provide an overview of the use of Ru^{II} alkynyl derivatives toward the understanding and the development of various research domains, ranging from nonlinear and linear optics to nano-and molecular electronics through molecular switches.

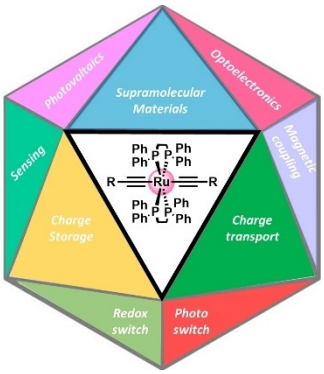

S. Rigaut, O. Galangau**